Electronic Supplementary Material (ESI) for Journal of Materials Chemistry C.

Supporting Information for

Putting Xenon and Nitrogen under Pressure: Towards New Layered and Two-Dimensional Nitrogen Allotropes with Crown Ether-like Nanopores

Busheng Wang‡, Frédéric Guégan‡, and Gilles Frapper*‡*

‡ Applied Quantum Chemistry group, E4 team, IC2MP UMR 7285, Université de Poitiers - CNRS, 4, rue Michel Brunet TSA 51106 - 86073 Poitiers Cedex 9, France. E-mail : wangbs123@gmail.com; gilles.frapper@univ-poitiers.fr

Contents

S1. Methodology details

S1.1 Evolutionary algorithm (USPEX)

We provide here the technical details of the USPEX evolutionary structural searches with a brief description of the fixed-composition evolutionary algorithm (EA). USPEX[1–4] (Universal Structure Predictor: Evolutionary Xtallography, version 10.4) is a global evolutionary search algorithm for structure prediction developed by the A.R. Oganov laboratory since 2004 (see http://uspex-team.org/en/uspex/overview). In this work, this EA code is interfaced with VASP[5,6] (Vienna Ab initio Simulation Package, version 5.4.4) for DFT structure relaxation (shape, volume, and atomic positions are optimized by VASP). To identify stable ground-state structures and compositions within the binary Xe−N system and other Ng-N binary systems (Ng = He, Ne, Ar, and Kr), a variable-composition evolutionary algorithm (VC-EA) implemented in the USPEX code is employed. It allows us to scan the configurational, structural, and composition spaces of XeN_x (where x is positive integer) and seek the local minima on the potential energy surface (PES). The VC-EA is performed at given pressures, in this case, 25, 50, 75 and 100 GPa. Finally, fixed composition EA (FC-EA) structural searches are undertaken for the given (x, y) compositions and pressures to ensure that the proposed structures are indeed the lowest in energy on the PES. The total number of atoms in the primitive cell is up to 44 for FC-EA searches, unless stated otherwise. One-hundred candidate structures are randomly produced in the first generation, and all subsequent generations contain 80 structures.

A structure is removed from the pool according to its fitness, that is the computed free enthalpy derived from *ab initio* total energy calculations (VASP). The remaining structures form the parent structures which participate in producing the next generation. Thus, a new candidate structure is produced from parent structures using one of four operators: (i) heredity (50%), (ii) permutation (10%), (iii) lattice mutations (10%), and (iv) softmutation (10%). Thus, 80% of the new candidates are generated from these evolutionary operators, while 20% were produced randomly. The USPEX search is done when

the global structure minimum is found in the last 10 generations. For a USPEX EA search, the number of generations is about 15-50. As mentioned previously, structure relaxations and energy calculations are done by the external code VASP (5 INCAR files, 5 steps per phase). Each fixed-composition USPEX job is run at least twice to ensure convergence to a global minimum.

S1.2 DFT computational details

DFT framework of USPEX calculations. First-principles calculations are performed using the projected-augmented-wave (PAW) method[7,8] as implemented in VASP (version 5.4.4). In USPEX calculation, exchange-correlation energy is treated using Perdew-Burke-Ernzerhof (PBE)[9,10], within the generalized gradient approximation (GGA) PAW potentials for xeon and nitrogen atoms have a radius of 2.0 au for Xe and 1.5 au for N ([He] core), respectively. Pseudopotentials with $4d^{10}5s^{2}5p^{6}$ and $2s^{2}2p^{3}$ valence configurations are employed for Xe and N, respectively.

To optimize each crystalline structure, 5 successive steps of increasing convergence accuracy are usually required (*i.e.*, 5 INCAR files). An illustration of this local optimization procedure is given in the PhD manuscript of B. Huang, "Computational materials discovery: prediction of carbon dioxide and nitrogen-based compounds under pressure using density functional theory and evolutionary algorithm", supervised by Pr. G. Frapper, IC2MP, Poitiers University (France), Dec. 2017 http://theses.univ-poitiers.fr/notice/view/59262). The parameters and criteria associated with VASP calculations then correspond to the last (5th) step, with the highest accuracy. A kinetic cutoff energy of 1000 eV is used for the wavefunction expansion with a Monkhorst-Pack k mesh grid with a spacing of $2\pi \times 0.03$ Å^{-1}. All structures are optimized until the net forces on atoms are below 1 meV/Å, resulting in enthalpies that converged to better than 1 meV per atom (lower than a chemical accuracy of 1 kcal/mol, *i.e.*, 0.04 eV/atom), and all forces on atoms are converged to less than 0.005 eV/Å. Then, the lowest ground-state (meta)stable phases obtained at the PBE level of theory are selected. For the two-dimensional systems,

we set a sufficiently large vacuum space to avoid interactions between neighboring images (vacuum ~15 Å).

Post-USPEX treatment: optimization

To fully optimize the selected phases, we tested other functionals. We finally chose to treat the weak dispersion forces of molecular structures (and others) through the inclusion of the revised Vydrov–van Voorhis nonlocal correlation (rVV10)[11,12] and used the strongly constrained and appropriately normed (SCAN) meta-GGA functional.[13] In this work, all the structural and energy values are discussed based on SCAN+rVV10 functional. For phonon calculations and *ab initio* molecular dynamics simulations, DFT-D3[14] correction was used instead of SCAN+rVV10, to take the vdW interactions into account with affordable computational resources.

Post-USPEX treatment: electronic structure, band gap and chemical bonding analysis

To perform chemical bonding analysis, we carried out single-point calculations at the SCAN+rVV10 level (using the geometries obtained from VASP) to calculate the density of states (DOS). Moreover, DFT-D3 correction was used in all phonon calculations and *ab initio* molecular dynamics simulations. SCAN has proven to be accurate for the description of structural properties of materials. In contrast, it may underestimate the value of the band gap. Therefore, we calculate the band gap (Eg) at the Heyd−Scuseria−Ernzerhof (HSE06)[15] hybrid functional level of theory, using the optimized SCAN+rVV10 structure (single-point energy calculation). This level of theory is noted thereafter as HSE06//SCAN+rVV10.

To further probe the electronic interaction between the subunits constituting the crystal structures (*e.g.*, Xe atoms and N_{20} matrix in XeN_{20}, we conducted additional single point calculations for each separated subunit, in the geometry, they adopt in the optimized structures, and computed the electron

density reorganization associated to the formation of the XeN_x crystal structures from the separated subunits,

$$\Delta\rho(r) = \rho(r) - \sum_{subunits} \rho_{subunit}(r)$$

We then plotted the associated isodensity maps (cf section S7). Non-zero values indicate the electron density in the XeN_x structure deviates from the simple superimposition of subunit densities, hence may probe charge transfer between subunits as well as intra-subunit polarization. Δρ calculations and plots were managed using VESTA.[16]

To complement this analysis, we additionally computed the Non-Covalent Interactions Index (NCI)[17,18] using the critic2 code,[19,20] working with CHGCAR files from VASP. NCI analysis relies on the fact that non-covalent interactions are expected to occur in regions where both the electron density and its (reduced) gradient are low valued; hence a study of regions displaying low values of both quantities should help in identifying interaction patterns. Inclusion of the second-order derivative of the electron density further helps in discriminating the type of interactions: depending on the sign of the second-highest Hessian eigenvalue, the interactions are stabilizing (<0, e.g. hydrogen bonds), repulsive (>0, e.g. steric clash) or weakly attractive (~0, e.g. van der Waals). NCI visualization (reduced electron density gradient isosurfaces multiplied by the sign of the second Hessian eigenvalue) was made using VMD scripts[21] (critic2 output).

Table S1: The different levels of theory employed and the properties computed in this work (√ stands for done, and x for undone).

Functionals	USPEX searches	Structural optimization	Single point energy	Electronic properties	Dynamical stability (Phonon)	Kinetic stability (AIMD)
PBE[9]	√	√	×	×	×	×
DFT-D3[14]	×	√	√	×	√	√
SCAN+rVV10[11–13]	×	√	√	√	×	×
HSE06[15]// SCAN+rVV10	×	×	√	√	×	×

S1.3 AIMD simulations

Ab initio molecular dynamics (AIMD) within canonical *NVT* ensemble using the Nosé heat bath scheme were performed to evaluate the thermal stability of specific phases up to 2000 K for 12 ps with a time step of 1 fs, and we allowed 2 ps for thermalization and then extracted data from the last 10 ps. In such AIMD simulations, the Brillouin zone integration is restricted to the Γ point of the supercell, due to a high calculation cost.

S1.4 Phonon calculations

In this work, first-principles phonon calculations using the finite displacements method at a quasi-harmonic level are done using the open-source package PHONOPY[22] (https://atztogo.github.io/phonopy/). Supercell structures with or without displacements are created from a reference unit cell considering all possible crystal symmetry operations. In general, a 2 x 2 x 2 supercell is sufficient, but larger ones can be required to avoid unphysical imaginary frequencies. Force constants are calculated using the optimized structure (VASP).

S2. Structural parameters and energies

Table S2. Structural parameters of dynamically stable Noble-nitride phases (distances in Å, angles in °, energy in eV/atom) at the SCAN+rVV10 level of theory.

Phase	Pressure (GPa)	Space group	Z	Lattice parameters	Atomic coordinates (fractional)
XeN_{20}	100	*Fm*-3	4	a=b=c=8.037 α=β=γ=90.0	Xe (0.000, 0.000, 0.500); N (0.000, 0.217, 0.170), (0.141, 0.141, 0.141)
XeN_{20}	0	*Fm*-3	4	a=b=c=8.673 α=β=γ=90.0	Xe (0.000, 0.000, 0.500); N (0.000, 0. 171, 0.211), (0.138, 0.138, 0.138)
XeN_{18}	100	*P*-1	1	a=5.452, b=5.446, c=5.009 α=110.1, β=94.9, γ=60.6	Xe (0.000, 0.000, 0.000); N (0.321, 0.350, 0.258), (-0.342, -0.322, 0.239), (0.078, -0.458, 0.214), (-0.378, -0.068, 0.247), (-0.466, 0.388, 0.258), (-0.099, 0.487, 0.291), (0.357, 0.102, 0.272), (0.442, -0.354, 0.245), (-0.060, 0.101, 0.466)
XeN_{16}	100	*P*-1	1	a=4.671, b=5.418, c=5.469 α=119.2, β=100.0, γ=104.6	Xe (0.000, 0.000, 0.000); N (0.222, 0.804, 0.411), (0.245, 0.519, 0.999), (0.266, 0.072, 0.640), (0.267, 0.609, 0.468), (0.277, 0.249, 0.553), (0.291, 0.795, 0.185), (0.339, 0.516, 0.788), (0.343, 0.736, 0.750)
XeN_8	100	*P*-1	1	a=5.452, b=5.230, c=2.599 α=80.6, β=78.4, γ=114.7	Xe (0.000, 0.000, 0.000); N (0.049, 0.373, 0.156), (0.119, 0.093, -0.485), (0.414, -0.472, -0.098), (0.333, 0.667, 0.222)
XeN_8	0	*P*6/*m*	1	a=b= 5.886, c=4.796 α=β=90.0, γ=120.0	Xe (0.000, 0.000, 0.000); N (0.083, -0.379, 0.500), (0.333, 0.667, 0.500)
XeN_4	25	$I4_1/amd$	4	a=b=5.330, c=8.930 α=β=γ=90.0	Xe (0.000, 0.250, 0.375); N (0.000, -0.025, -0.060)
XeN_4 [23]	18.7	$I4_1/amd$	4	a=b= 5.723, c= 9.213 α=β=γ=90.0	Xe (0.000, 0.250, 0.375); N (0.000, -0.025, -0.060); N (0.5, 0.721, 0.719)
XeN_4 [24]	10.3	$I4_1/amd$	4	a=b= 5.982, c= 9.338 α=β=γ=90.0	Xe (0.000, 0.250, 0.375); N (0.000, -0.025, -0.060) [0.238, 0.252, 0.809] [0.272 , 0.229, 0.687]
XeN_4	5	$I4_1/amd$	4	a=b=6.241, c=10.057 α=β=γ=90.0	Xe (0.000, 0.250, 0.375); N (0.000, 0.023, -0.446)
XeN_4 [23,24] $Xe(N_2)_2$	5.6	*Fd*-3*m* Cu_2Mg-type	2	a=b=c=9.236 α=γ=β=90.0	Xe (0.000, 0.000, 0.000); N_2 (0.625, 0.125, 0.125)

XeN_4 was identified as an *Fd*-3*m* structure $Xe(N_2)_2$ at ~ 5 GPa in previous experimental studies,[23,24] the authors treated the freely rotating N_2 molecules as units during the symmetry analysis. It's convenient and easy to understand the crystal structure, however, the XeN_4 is not a real *Fd*-3*m* structure.

Table S3. Calculated enthalpies of the predicted XeN_x compounds at different pressure.

Structure	Space Group	Pressure (GPa)	Enthalpy (eV/atom)			Formation Enthalpy (eV/atom)		
			PBE	D3	SCAN+ rVV10	PBE	D3	SCAN+ rVV10
Stable								
XeN_4	$I4_1/amd$	5	-5.929	-6.035	-13.816	-0.004	-0.017	-0.016
XeN_8	P-1	100	-0.782	-0.932	-5.622	-0.286	-0.283	-0.236
XeN_{18}	P-1	100	-1.873	-2.007	-4.688	-0.267	-0.260	-0.216
XeN_{20}	Fm-3	100	-1.949	-2.085	-4.598	-0.248	-0.244	-0.204
Metastable								
XeN_{16}	P-1	100	-1.705	-1.859	-4.731	-0.216	-0.229	-0.173
Quenchable								
XeN_{20}	Fm-3	0	-6.291	-6.408	-8.867	1.643	1.573	1.577
XeN_{16}	P-1	0	-6.530	-6.916	-9.729	1.312	0.973	1.012
XeN_8	$P6/m$	0	-6.589	-6.551	-11.163	0.823	0.910	0.960

Table S4. Structural parameters and relative enthalpy of several nitrogen allotropes @ 0 GPa (distances in Å, angles in °, energy in eV/atom) at the SCAN+rVV10 level of theory. N indicates the number of atoms in each unit cell.

Phase	Relative E	Space group	N	Lattice parameters	Atomic coordinates (fractional)
ε-N_2	0.000	*R*-3*c*	48	a=b=8.595, c=12.104 α=β= 90.0, γ=120.0	N (0.000, 0.000, 0.454), (0.058, 0.790, 0.721)
α-N_2	-0.016	*Pa*-3	8	a=b=c=5.222 α=β=γ=90.0	N (0.061, 0.061, 0.061)
cg-$N^{25,26}$	1.368	$I2_13$	8	a=b=c=5.222 α=β=γ=90.0	N (0.166, 0.166, 0.166)
N_8^{27}	0.902	*P*1	16	a=4.406, b=6.436, c=7.467 α=99.6, β=99.9, γ=91.1	N (0.037, 0.619, 0.871), (0.057, 0.011, 0.150), (0.149, 0.474, 0.981), (0.228, 0.062, 0.728), (0.274, 0.010, 0.256), (0.410, 0.542, 0.072), (0.450, 0.072, 0.831), (0.513, 0.391, 0.177), (0.516, 0.045, 0.375), (0.564, 0.504, 0.670), (0.610, 0.856, 0.434), (0.769, 0.440, 0.277), (0.787, 0.546, 0.771), (0.847, 0.871, 0.553), (0.989, 0.076, 0.613), (0.994, 0.448, 0.379)
LP-N^{28}	1.573	*Pba*2	16	a=b=4.618, c=5.257 α=β=γ=90.0	N (0.005, 0.329, 0.236), (0.171, 0.995, 0.763), (0.239, 0.743, 0.631), (0.241, 0.757, 0.369)
t-N_4^{29}	1.532	$I4_1/a$	16	a=b=5.369, c=3.818 α=β=γ=90.0	N (0.129, 0.295, 0.057)
N_{10}^{30}	0.807	$P2_1$	10	a=5.015, b=5.934, c=8.268 α=γ=90.0, β=103.3	N (0.018, 0.387, 0.270), (0.077, 0.717, 0.654), (0.103, 0.929, 0.022), (0.121, 0.174, 0.470), (0.128, 0.986, 0.869), (0.272, 0.450, 0.345), (0.289, 0.046, 0.119), (0.328, 0.133, 0.870), (0.336, 0.317, 0.470), (0.427, 0.170, 0.026)
N_{10}^{31}	1.388	$P6_3/m$	10	a=b=5.687, c=5.366 α=β=90.0, γ=120.0	N (0.086, 0.812, 0.523), (0.115, 0.704, 0.750), (0.333, 0.667, 0.750)
BP-$N^{32,33}$	1.470	*Cmce*	8	a=2.220, b=7.610, c=3.263 α=β=γ=90.0	N (0.000, -0.411, -0.377)
N_{20}[a]	1.384	*Fm*-3	40	a=b=c=8.417 α=β=γ=90.0	N (0.000, 0.221, 0.166), (0.140, 0.140, 0.140)
3D-N_8 [a]	1.031	*P*-1	8	a=4.093, b=4.961, c=4.208 α=79.3, β=89.7, γ=80.2	N (0.174, -0.323, -0.326), (-0.026, -0.075, -0.368), (-0.431, 0.374, -0.474), (0.132, 0.468, -0.073)
2D-N_8 [a]	1.080	*P*-3	8	a=b=5.880, c=15.425 α=β=90.0, γ=120	N (0.333, 0.667, 0.500), (-0.463, -0.381, 0.500)

[a]This work.

Table S5. Enthalpies and structural parameters of Nitrogen and Xenon elements at selected pressures (distances in Å, angles in °, energy in eV/atom) at the SCAN+rVV10 level of theory.

Phase	E	P	Space Group	Lattice Parameters	Atomic coordinates (fractional)
Xe	-35.617	0	*Fm*-3*m*	a=b=c=6.037 α=β=γ=90.0	Xe (0.000, 0.000, 0.000)
Xe	-34.195	5	*Fm*-3*m*	a=b=c=5.426 α=β=γ=90.0	Xe (0.000, 0.000, 0.000)
Xe	-30.082	25	*Fm*-3*m*	a=b=c=4.879 α=β=γ=90.0	Xe (0.000, 0.000, 0.000)
Xe	-26.012	50	*Fm*-3*m*	a=b=c=4.608 α=β=γ=90.0	Xe (0.000, 0.000, 0.000)
Xe	-22.480	75	$P6_3/m$	a=b=3.135, c=5.136 α=β=90.0, γ=120.0	Xe (0.333, 0.667, 0.250)
Xe	-19.273	100	$P6_3/m$	a=b=3.047, c=4.999 α=β=90.0, γ=120.0	Xe (0.333, 0.667, 0.250)
N	-9.187	0	*Pa*-3[a]	a=5.856, b=5.856, c=5.856 α=90.0, β=90.0, γ=90.0	N (0.055, 0.055, 0.055)
N	-8.685	5	*R*-3*c*	a=b=8.008, c=12.104 α=β= 90.0, γ=120.0	N (0.000, 0.000, 0.451), (0.061, 0.790, 0.721)
N	-7.311	25	*R*-3*c*	a=b=7.240, c=11.164 α=β= 90.0, γ=120.0	N (0.000, 0.000, 0.446), (0.063, 0.463, 0.882)
N	-5.935	50	*R*-3*c*	a=b=6.849, c=9.648 α=β= 90.0, γ=120.0	N (0.000, 0.000, 0.443), (0.064, 0.466, 0.878)
N	-4.740	75	*R*-3*c*	a=b=6.559, c=9.305 α=β= 90.0, γ=120.0	N (0.000, 0.000, 0.441), (0.065, 0.469, 0.876)
N	-3.658	100	*R*-3*c*	a=b=6.342, c=9.093 α=β= 90.0, γ=120.0	N (0.000, 0.000, 0.440), (0.068, 0.472, 0.874)
N	-7.323	25	$P4_12_12$	a=b=3.000, c=8.454 α=β=γ=90.0	N (0.057, 0.814, 0.523)
N	-5.956	50	$P4_12_12$	a=b=2.834, c=7.949 α=β=γ=90.0	N (0.064, 0.807, 0.524)
N	-4.940	75	$I2_13$	a=b=c=3.552 α=β=γ=90.0	N (0.174, 0.174, 0.174)
N	-4.083	100	$I2_13$[b]	a=b=c=3.501 α=β=γ=90.0	N (0.176, 0.176, 0.176)

[a] Molecular crystal (N-N = 1.11 Å in triple bonded N_2); [b]3D covalent net (N-N = 1.34 Å, 3-coordinated N, 10-rings).

Table S6. Selected parameters for bonding analysis in XeN_x phases: interatomic separations, van der Waals radii, and electronegativities.

Pressure (GPa)	0	25	100
Interatomic separation [a] (Å)			
d(N≡N) triple bond [b]	1.11	-	-
d(N=N) double bond [c]	1.36	-	-
d(N-N) single bond [d]	1.41	1.38	1.34
d(Xe-Xe)	4.27 [e]	3.45 [e]	3.06 [f]
van der Waals diameter [g] (Å)			
r_{vdW}(Xe-N)	4.11	3.02 [h]	2.70
r_{vdW}(Xe-Xe)	4.64	3.40 [h]	3.04
Electronegativity [g] (eV/e^{-1})			
χ (N)	16.85	15.81 [h]	14.01
χ (Xe)	14.95	13.64 [h]	11.48
δχ (Xe-N)	1.90	2.17 [h]	2.53

[a]SCAN+rVV10 level; [b]In molecular N_2; [c]In molecular HN=NH; [d]In *cg*-N phase; [e]In *fcc* (*Fm*-3*m*) Xe phase; [f]In *hcp* (*P*6$_3$/*m*) Xe phase; [g]The Atoms Under Pressure (AUP) database [19–22]; [h]at 24 GPa.

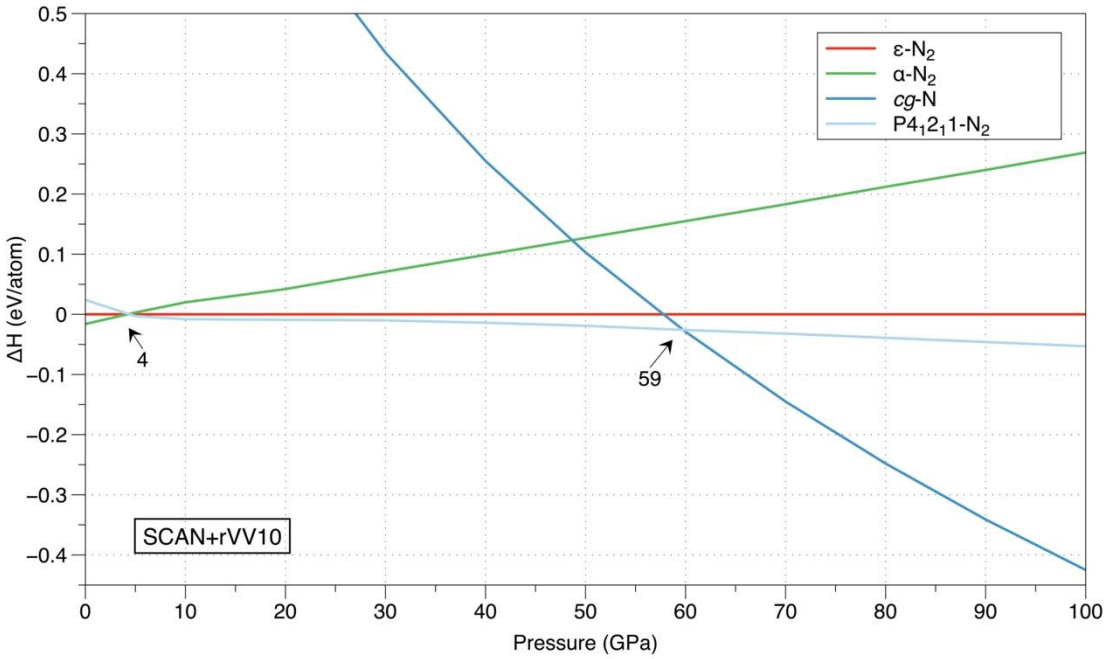

Figure S1. Relative enthalpies as a function of pressure for molecular nitrogen α-N_2 (*Pa*-3), ε-N_2 (*R*-3*c*), and *P*4$_1$2$_1$2-N_2, as well as the polymeric *cg*-N.

Clearly, α-N_2 is the ground stable phase at 0 GPa. When the pressure increases, α-N_2 transfers to *P*4$_1$2$_1$2-N_2 above ~4 GPa. In the pressure range from 4 to 59 GPa, the ε-N_2 is slightly above *P*4$_1$2$_1$2-N_2. Finally, the polymeric *cg*-N turns out to be the most stable phase above 59 GPa.

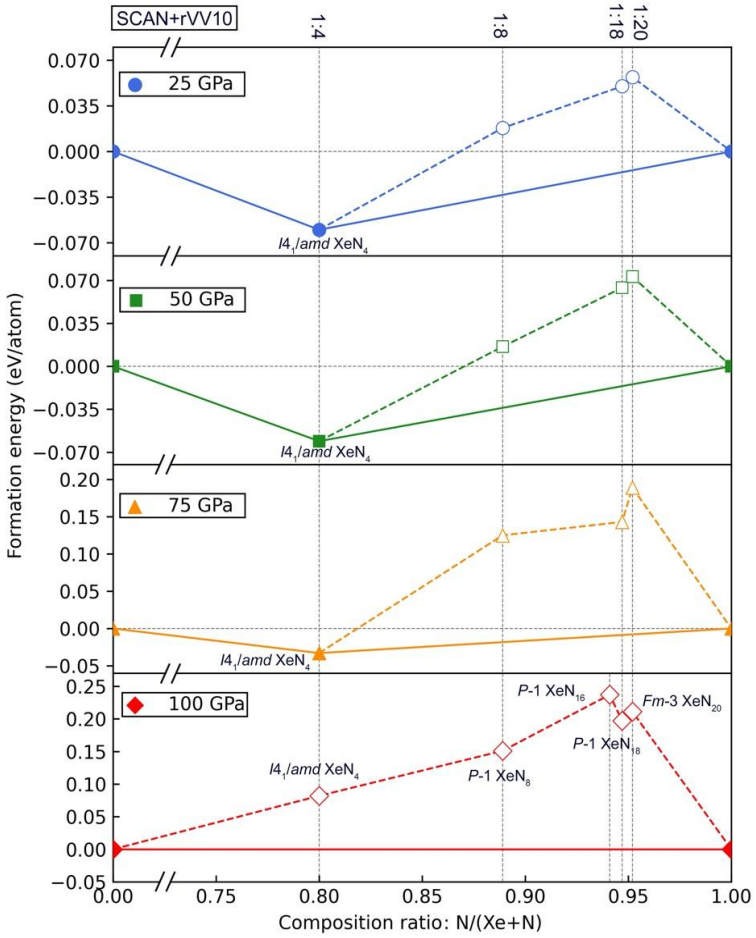

Figure S2. Convex-hull diagrams for the Xe−N system under selected pressure regarding the ground-state elements. $P4_12_12$-N_2 and *fcc* Xe at 25 and 50 GPa, while *cg*-N and *hcp* Xe at 75 and 100 GPa were used to calculate the formation enthalpies. Solid symbols denote stable structures, and empty ones represent metastable structures. The space group is indicated for each novel stable structure.

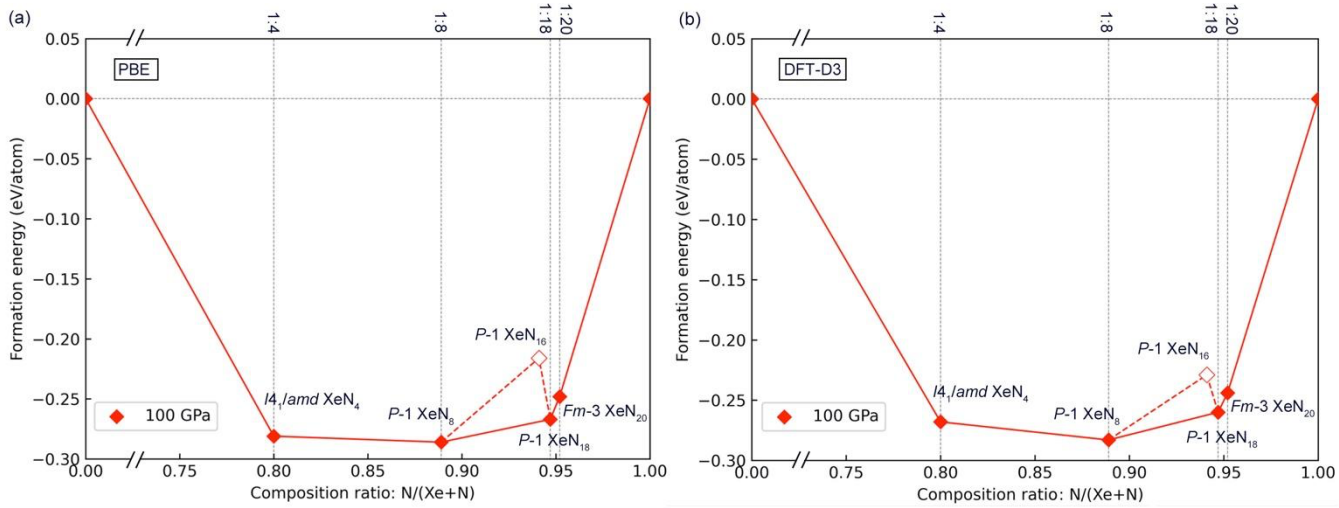

Figure S3. Convex-hull diagrams for the Xe−N system under 100 GPa regarding the hcp-Xe ($P6_3/m$) and ε-N_2 (R-3c) with (a) PBE and (b) DFT-D3 levels of theory. Solid symbols denote stable structures, and empty ones represent metastable structures. The space group is indicated for each novel stable structure.

As shown in Figure S3, the PBE and DFT-D3 moderately shift the stability figures, but the phase stability order is not changed.

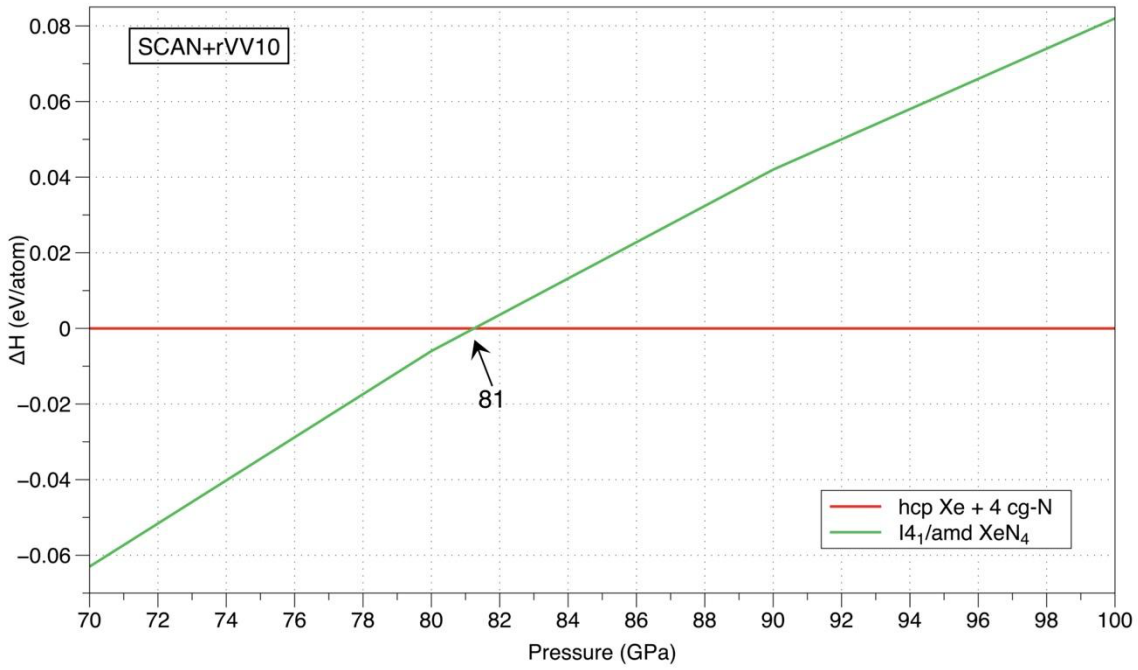

Figure S4. Calculated enthalpy curves of *I*4$_1$*/amd* XeN_4 with respect to *hcp* Xe and *cg*-N under pressure (SCAN+rVV10 level). *I*4$_1$*/amd* XeN_4 has a positive formation enthalpy above 81 GPa.

S3. Dynamical stability

a. Xenon nitrides

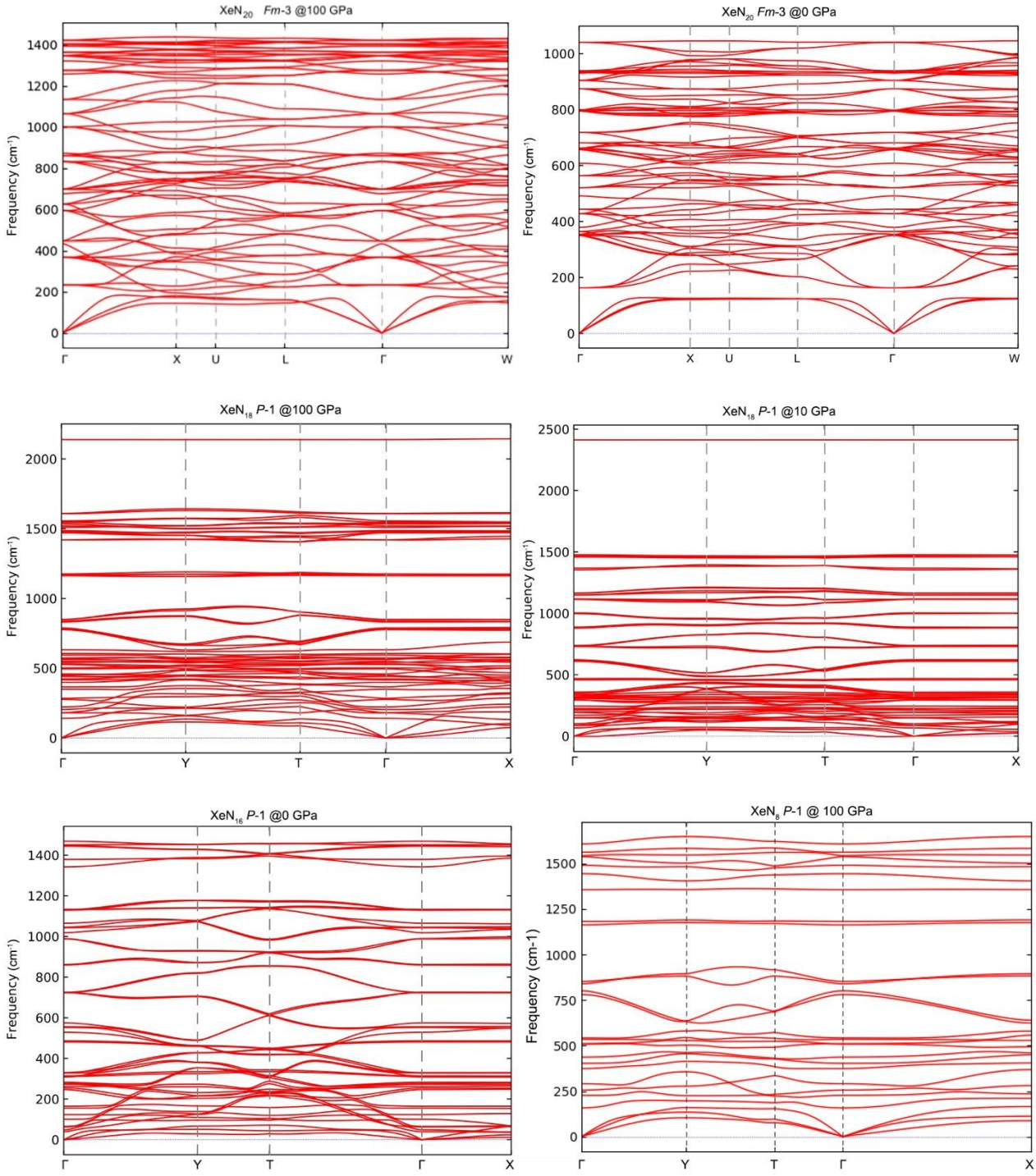

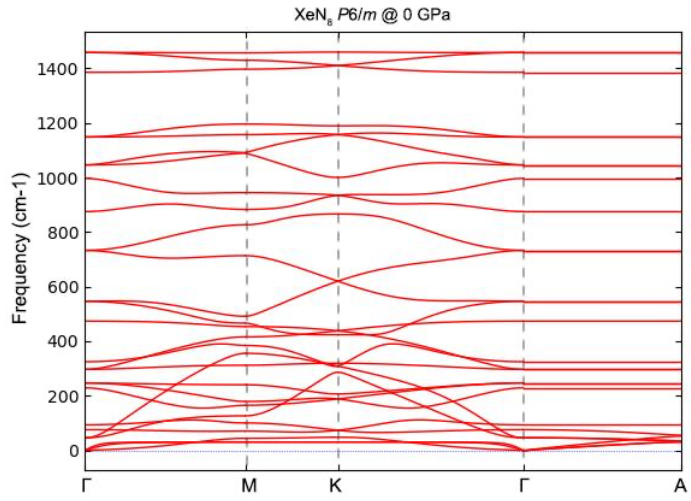

b. Polymeric nitrogen compounds (N_{20} and layered 3D and 2D N_8)

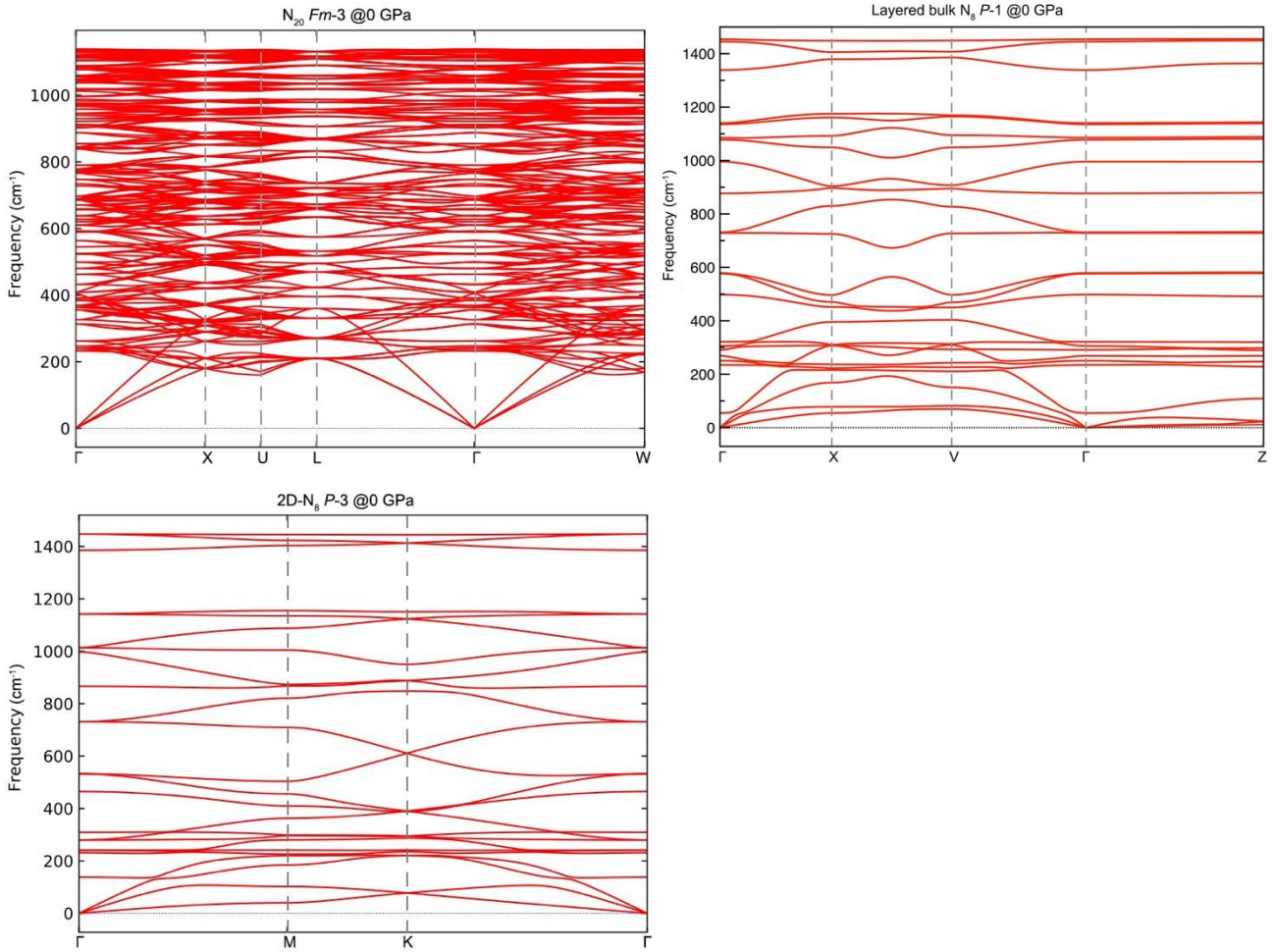

Figure S5. Phonon dispersion curves of XeN_{20}, XeN_{18} , XeN_8 and polymeric nitrogen compounds (N_{20} and N_8) at selected pressures (DFT-D3).

No imaginary phonon modes are found in the whole Brillouin zone. This confirms the dynamical stability of each phase.

S4. AIMD simulations

AIMD simulations with canonical ensemble using the Nosé heat bath scheme were performed to evaluate the thermal stability of specific phases up to 2000 K for 12 ps, see Figure S6-S12. Radial distribution functions (RDF) of specific phases are also presented, which reveal if the contacts between atoms (N-N, or Xe-N) are preserved at high temperatures.

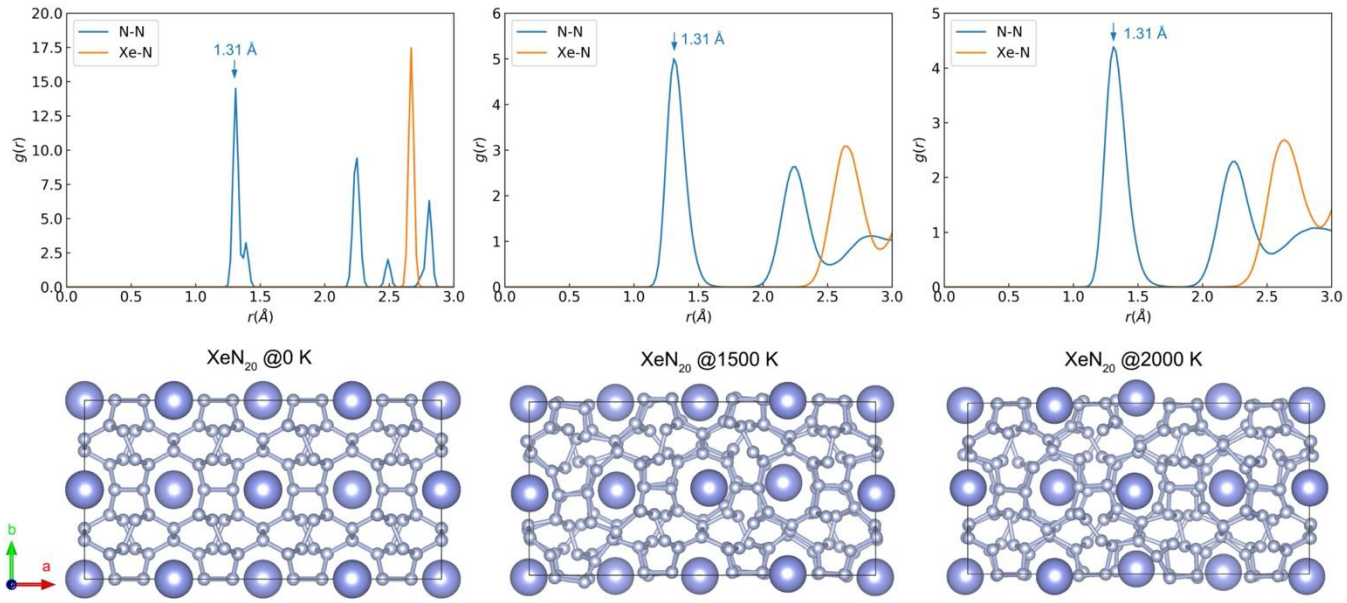

Figure S6. RDF (upper panel) and snapshots (lower panel) of the *Fm*-3 XeN_{20} at 100 GPa with 2 × 1 × 1 supercell (168 atoms) after 12 ps AIMD simulations at 0 K, 1500 K, and 2000 K, respectively. Large portage spheres are xenon atoms, and small gray spheres are nitrogen atoms. The single bonds N-N under 100 GPa (1.31 Å) are indicated by blue arrows in RDF.

These AIMD simulations demonstrate the single bonds N-N framework within XeN_{20} could be maintained up to 2000 K at 100 GPa.

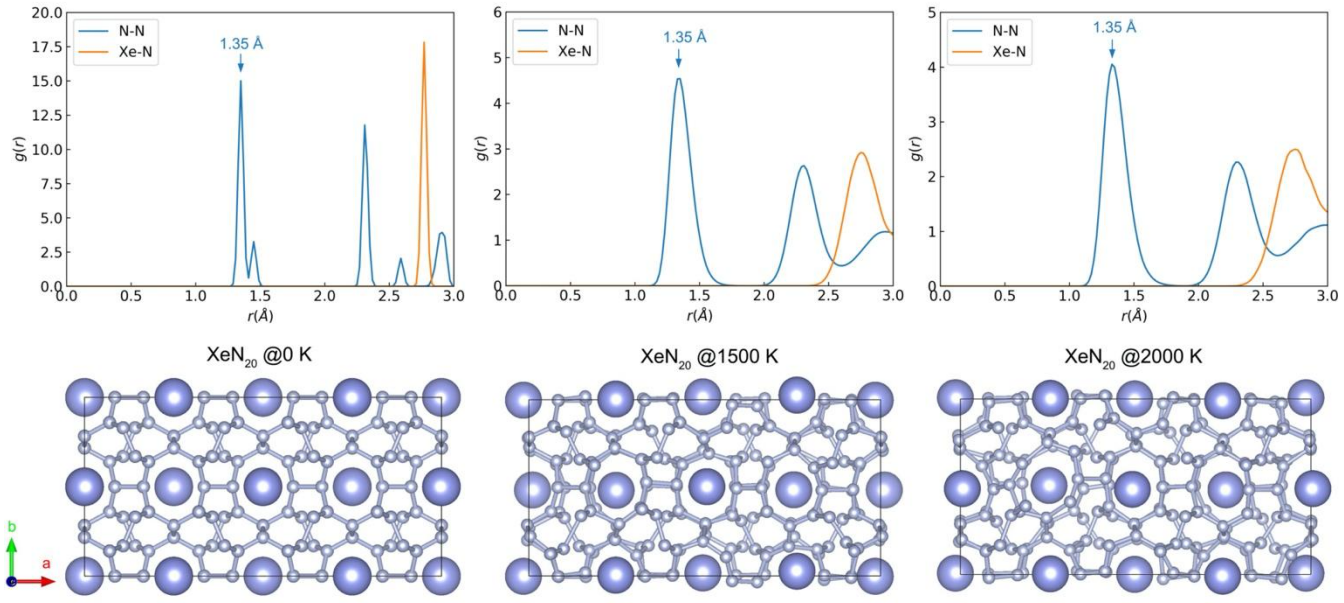

Figure S7. RDF (upper panel) and snapshots (lower panel) of the *Fm*-3 XeN_{20} at 50 GPa with 2 × 1 × 1 supercell (168 atoms) after 12 ps AIMD simulations at 0 K, 1500 K and 2000 K, respectively. The single bonds N-N under 50 GPa (1.35 Å) are shown by blue arrows in RDF.

These AIMD simulations analyses indicate that the single bonds N-N framework within XeN_{20} could be maintained up to 2000 K at 50 GPa.

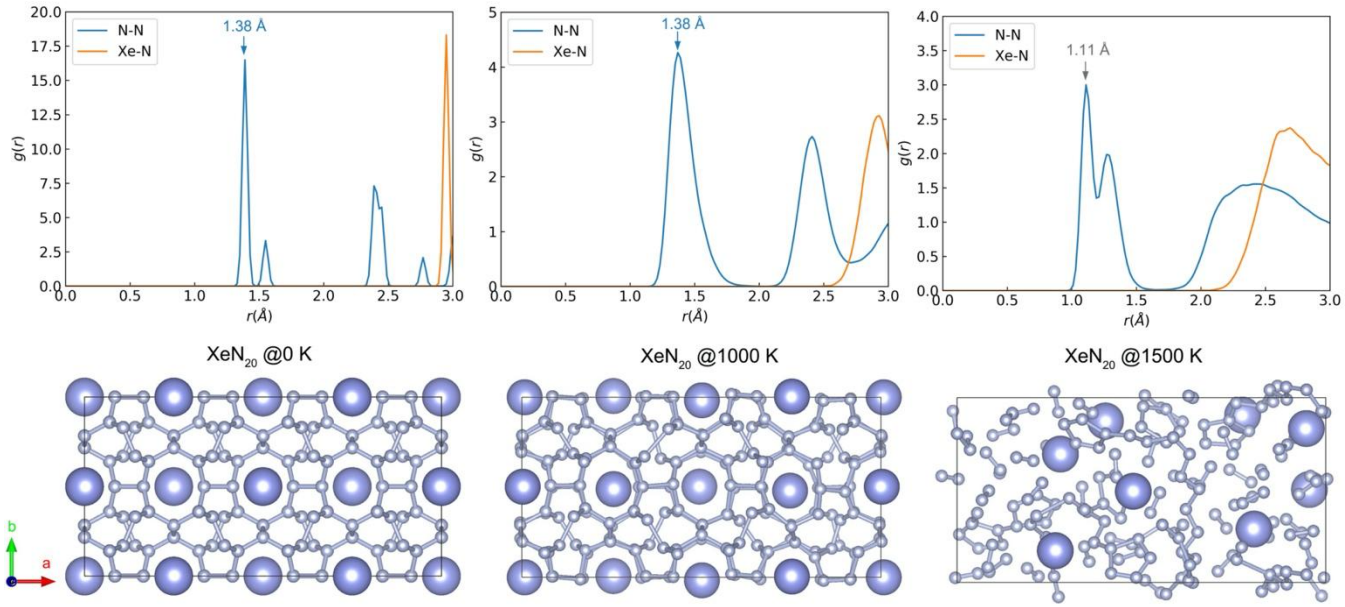

Figure S8. RDF (upper panel) and snapshots (lower panel) of the *Fm*-3 XeN_{20} at 0 GPa with 2 × 1 × 1 supercell (168 atoms) after 12 ps AIMD simulations at 0 K, 1000 K, and 1500 K, respectively. The single bonds N-N under 0 GPa (1.38 Å) are shown by blue arrows in RDF for 0 K and 1000 K.

The polymeric Nitrogen is crashed at 1500 K, and the signals for N_2 dimers (1.11 Å) are observed from both RDF and snapshots, which indicate the single bonds N-N framework within XeN_{20} could be maintained up to 1000 K, but will be crashed under 1500 K at 0 GPa.

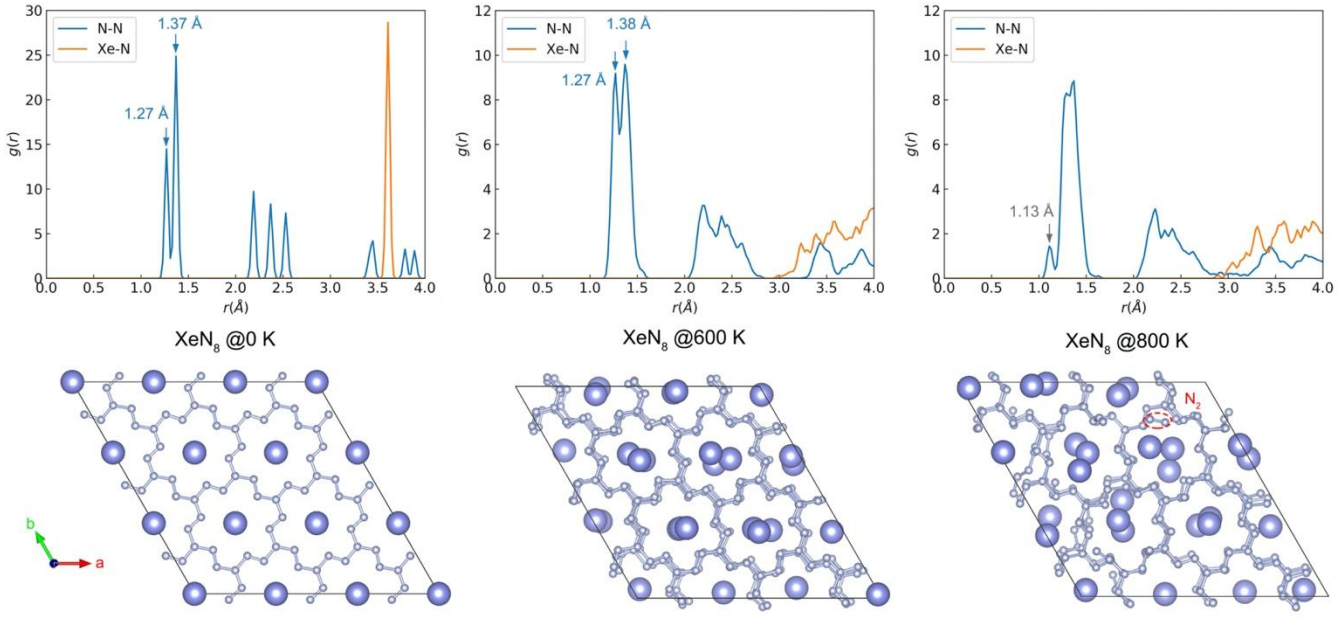

Figure S9. RDF (upper panel) and snapshots (lower panel) of the *P*6/*m* XeN_8 at 0 GPa with 3 × 3 × 3 supercells (243 atoms) after 12 ps AIMD simulations at 0 K, 600 K, and 800 K, respectively. The single bonds (1.27 Å) and double bonds (1.37 Å) N-N under 0 GPa are shown by blue arrows in RDF for 0 K and 600 K.

The polymeric Nitrogen is crashed at 800 K, and the signals for N_2 dimers (1.13 Å) are observed from both RDF and snapshots, which indicate the single bonds N-N framework within *P*6/*m* XeN_8 could be maintained up to 600 K, but will be crashed under 800 K at 0 GPa.

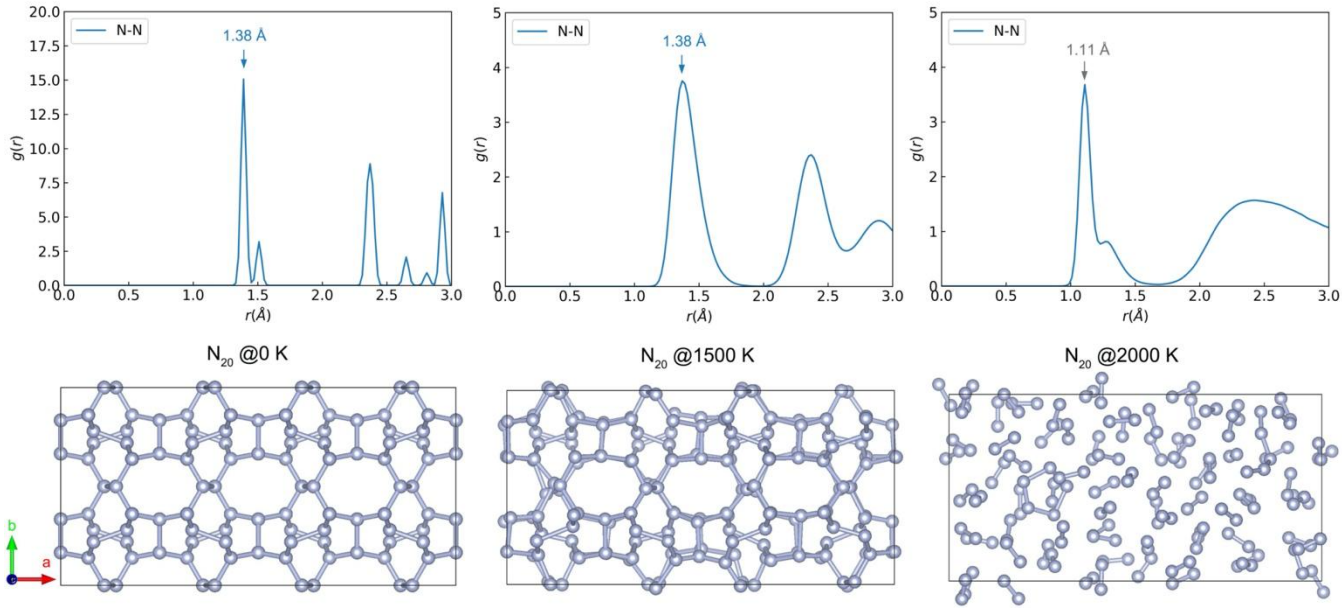

Figure S10. RDF (upper panel) and snapshots (lower panel) of the *Fm*-3 N_{20} at 0 GPa with 2 × 1 × 1 supercell (160 atoms) after 12 ps AIMD simulations at 0 K, 1500 K, and 2000 K, respectively. The single bonds N-N under 0 GPa (1.38 Å) are shown by blue arrows in RDF for 0 K and 1500 K.

The polymeric Nitrogen is crashed at 1500 K, and the signals for N_2 dimers (1.11 Å) are observed from both RDF and snapshots, which indicate the single bonds N-N framework within N_{20} could be maintained up to 1500 K, but will be crashed under 2000 K at 0GPa.

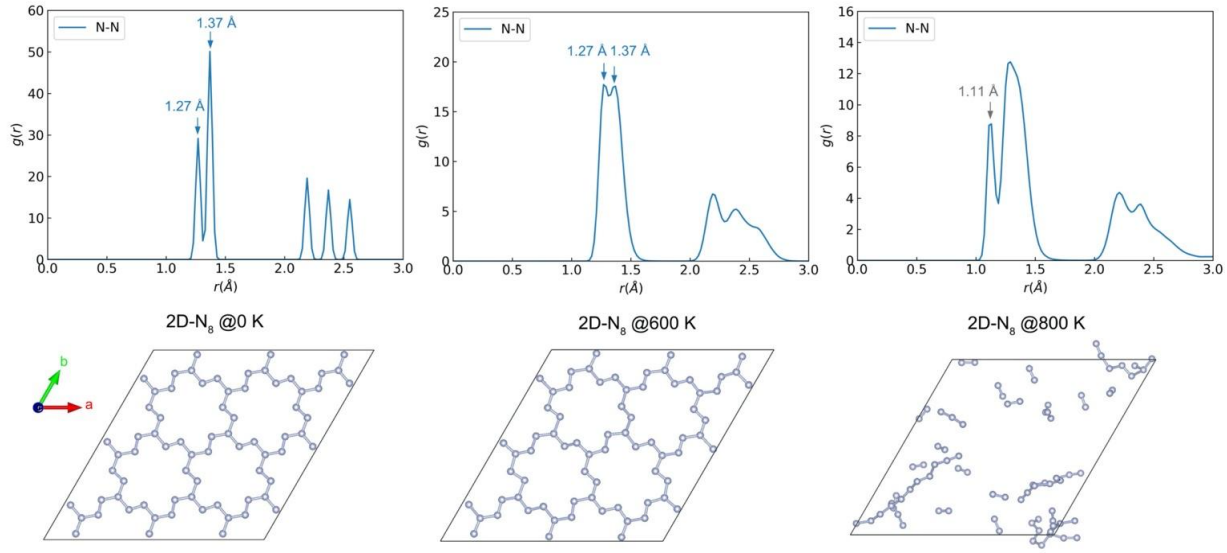

Figure S11. RDF (upper panel) and snapshots (lower panel) of the *P*-3 2D-N_8 at 0 GPa with 3 × 3 × 1 supercell (72 atoms) after 10 ps AIMD simulations at 0 K, 600 K, and 800 K, respectively. The single bonds (1.27 Å) and double bonds (1.37 Å) N-N under 0 GPa are shown by blue arrows in RDF for 0 K and 600 K.

The polymeric Nitrogen is crashed at 800 K, and the signals for N_2 dimers (1.11 Å) are observed from both RDF and snapshots, which indicate the single bonds N-N framework within 2D-N_8 could be maintained up to 600 K, but will be crashed under 800 K at 0 GPa.

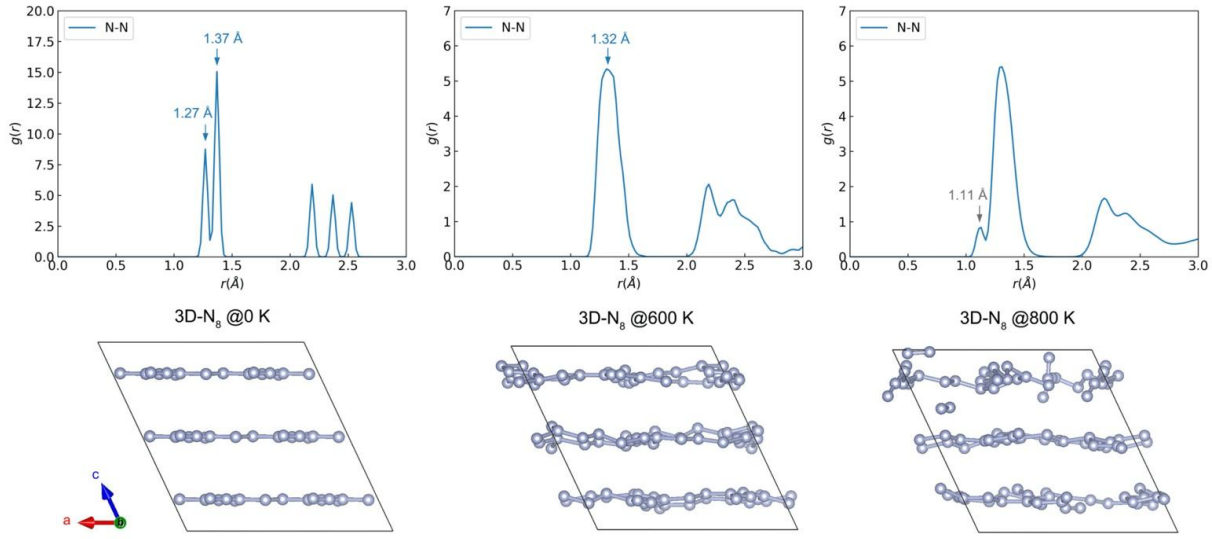

Figure S12. RDF (upper panel) and snapshots (lower panel) of the *P*-1 3D-N_8 at 0 GPa with 2 × 2 × 3 supercell (96 atoms) after 10 ps AIMD simulations at 0 K, 600 K, and 800 K, respectively. The single bonds (1.27 Å) and double bonds (1.37 Å) N-N under 0 GPa are shown by blue arrows in RDF for 0 K and 600 K.

The polymeric Nitrogen is crashed at 800 K, and the signals for N_2 dimers (1.11 Å) are observed from both RDF and snapshots, which indicate the single bonds N-N framework within 3D-N_8 could be maintained up to 600 K, but will be crashed under 800K at 0GPa.

S5. Electronic properties

a. Projected band structures and density of states (DOS) at SCAN+rVV10 level. The colored bands of band structures indicate the atomic contributions to the band structure, from red (high Xe contributions) to green (high N contribution).

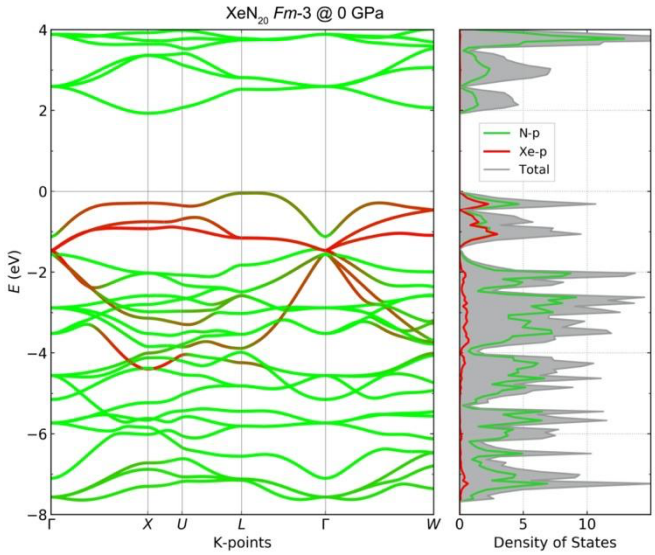

Figure S13. Band structure and DOS for *Fm*-3 XeN_{20} at 0 GPa.

A bandgap is observed for *Fm*-3 XeN_{20} at 100 and 0 GPa using SCAN+U+rVV10 functional.

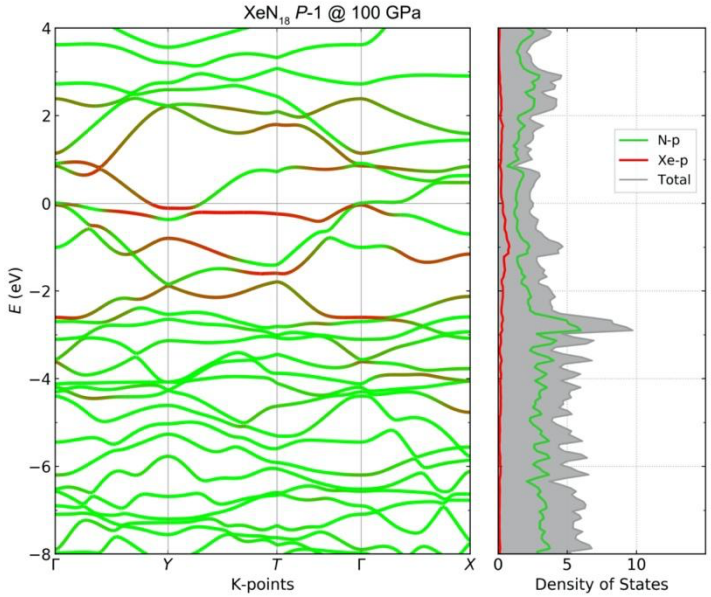

Figure S14. Band structure and DOS for *P*-1 XeN_{18} at 100 GPa.

Fermi level crosses the conductive bands, indicating that P-1 XeN18 is metallic at 100 GPa using SCAN+rVV10 functional.

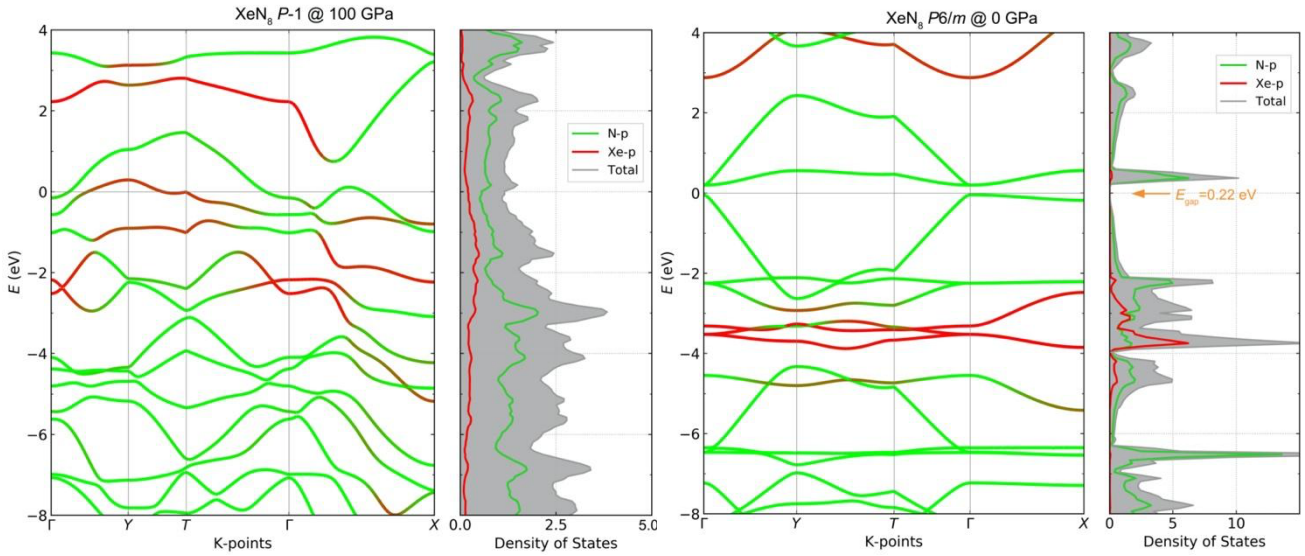

Figure S15. Band structure and DOS for *P*-1 XeN_8 at 100 GPa, and *P*6/*m* XeN_8 0 GPa.

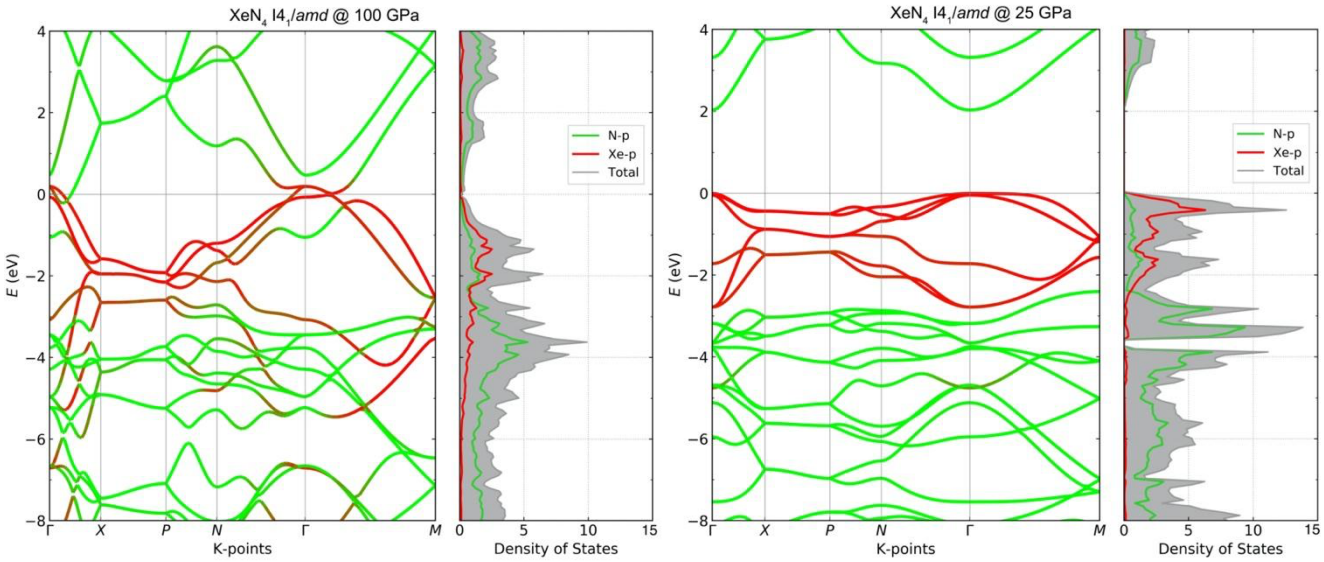

Figure S16. Band structure and DOS for *I*4$_1$/*amd* XeN_4 at 100 and 25 GPa.

The calculated metallic behavior of XeN_4 at 100 GPa has good agreement with the previous experimental report.[23,24]

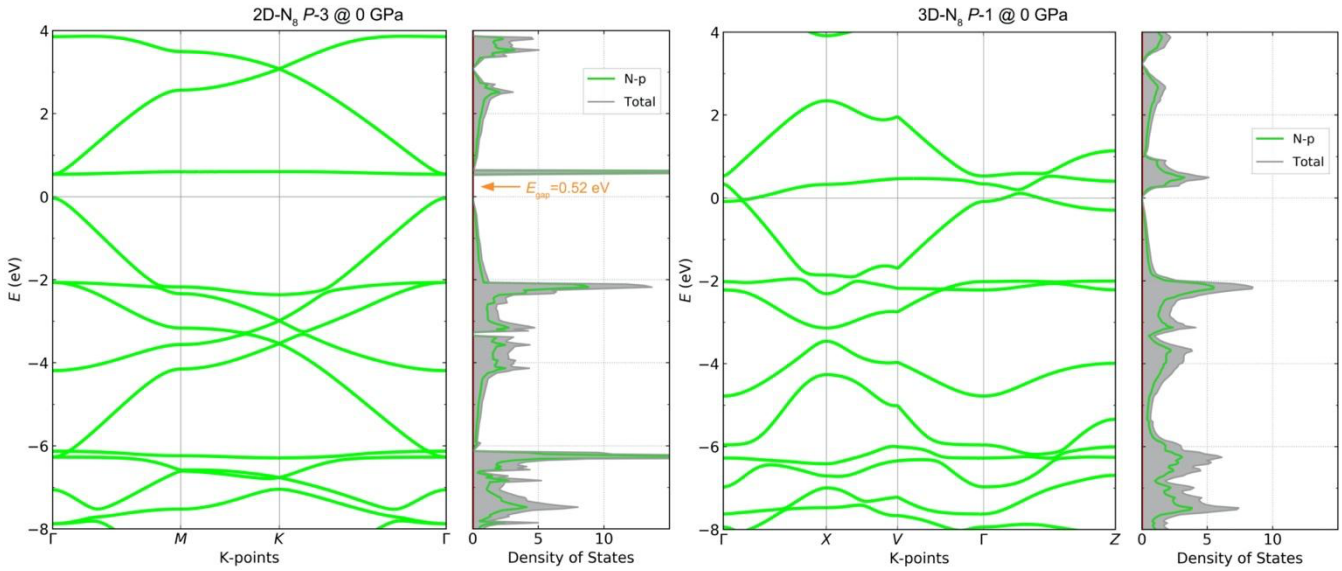

Figure S17. Band structure and DOS for *P*-3 2D-N_8 and *P*-1 3D-N_8 at 0 GPa.

b. Projected DOS-HSE06 at SCAN+rVV10 level.

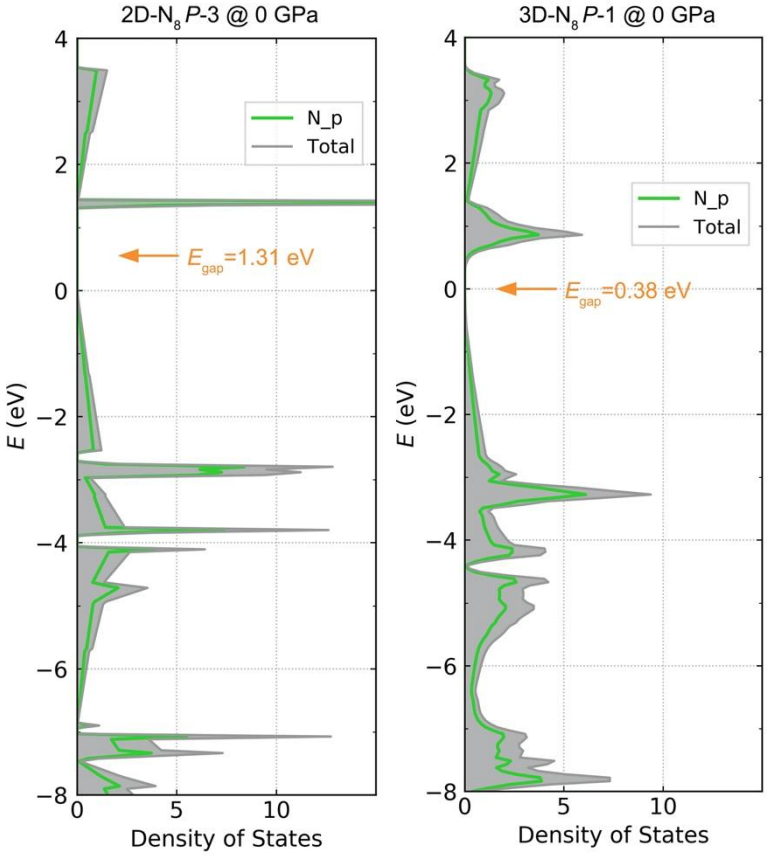

Figure S18. DOS computed with HSE06//SCAN+rVV10 showing band gap for both *P*-3 2D-N_8 (E_{gap} = 1.31 eV) and *P*-1 3D-N_8 (E_{gap} = 0.38 eV) at 0 GPa.

S6. Gibbs free energy of formation of XeN_{20}

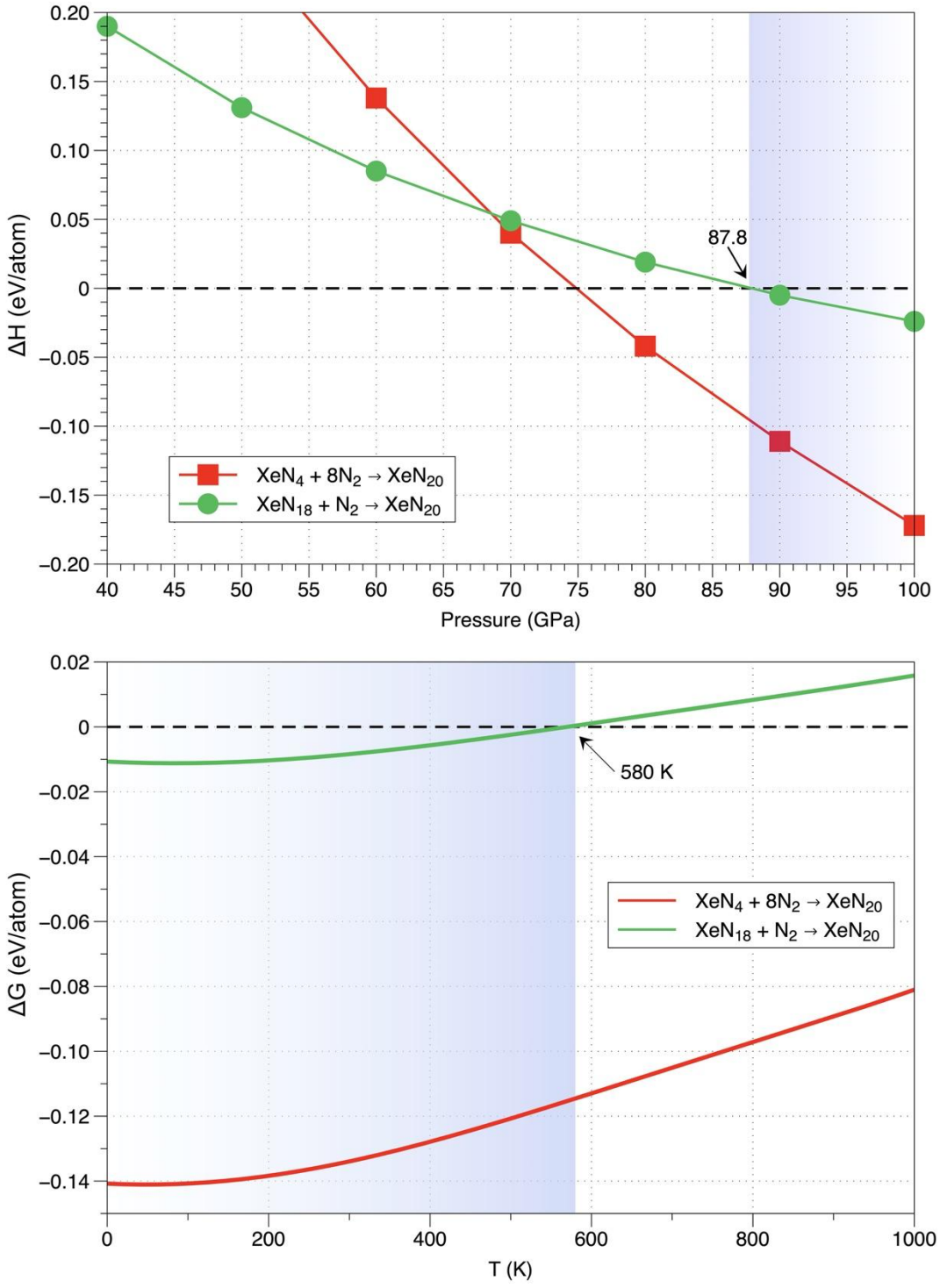

Figure S19. Relative enthalpies and Gibbs free energy of proposed reactions for $XeN_4+8N_2 \rightarrow XeN_{20}$ (red line) and $XeN_{18}+N_2 \rightarrow XeN_{20}$ (green line) with PBE functionals at high-pressure and high-temperature.

The calculations within DFT-D3 indicate that the XeN_{20} is stable at high pressure and high temperatures.

S7. Intermolecular interaction patterns in XeN_x (x = 4, 8, 18, and 20)

S7.1 Electron density reorganisation maps

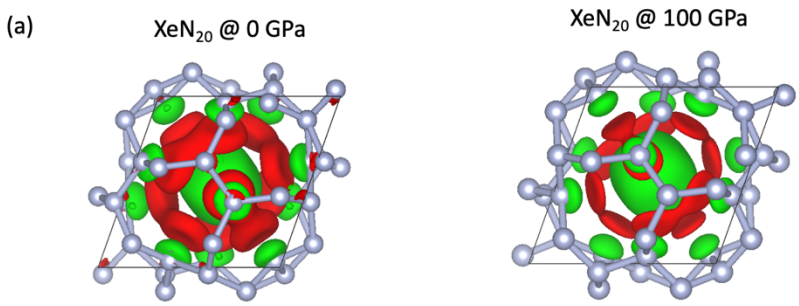

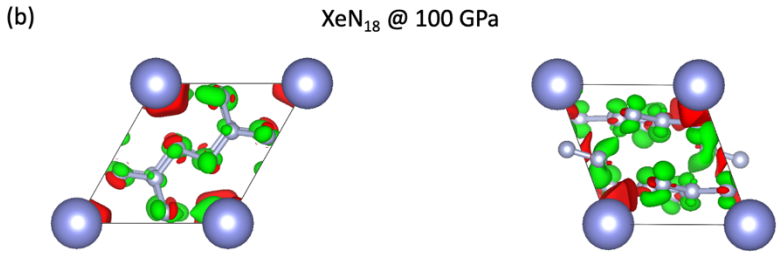

Left: view along *a*, right: view along *c*.

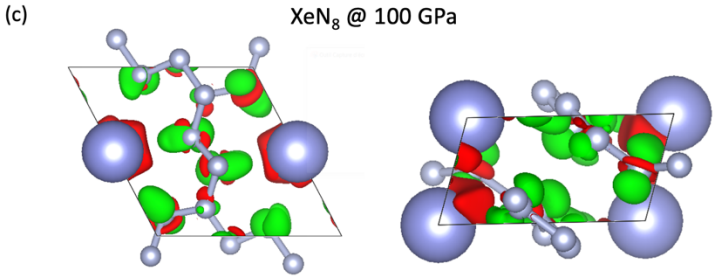

Left: view along a, right: view along c.

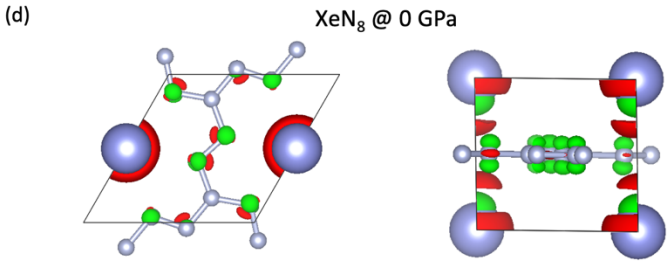

Left: view along a, right: view along c.

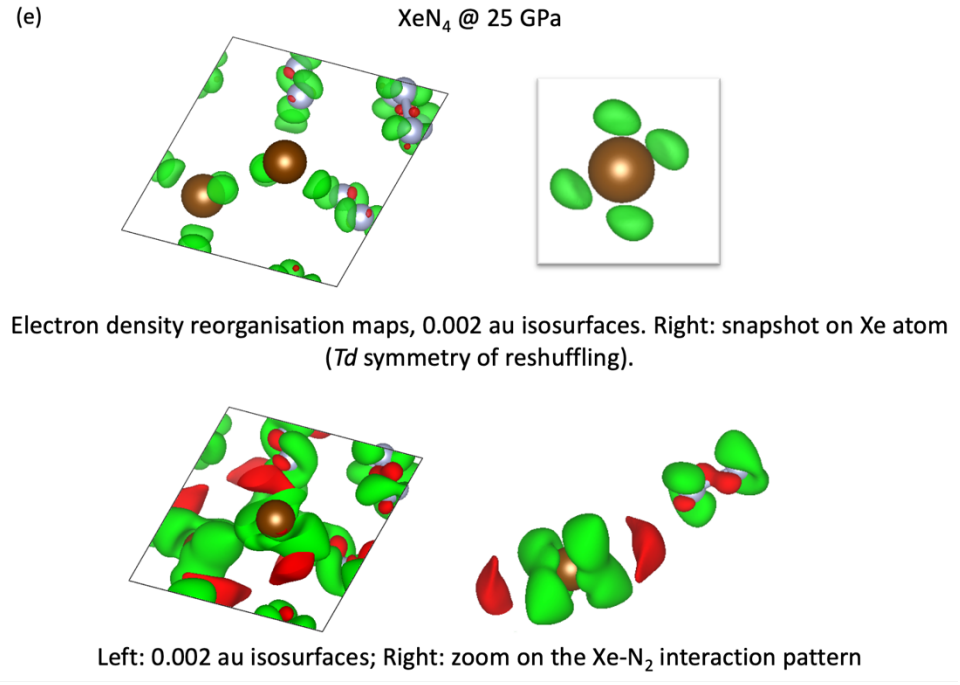

Figure S20. Electron density reorganization map with isosurface for XeN_4, XeN_8, XeN_{18}, and XeN_{20} under specific pressure. Red and green regions indicate depletion and accumulation of electrons, respectively.

As shown in Figure S20, in most cases both Xe and polynitrogen subunits display both negative and positive contributions of Δρ, which suggests each fragment is experiencing an electron density polarisation due to the interaction, rather than a genuine charge transfer. Nevertheless, the cases of XeN_{18} and XeN_8 at 100 GPa could indicate a slight charge transfer from the Xe atom to the N matrix (only depletion areas being visible on Xe atoms in these cases). It may be noted in the case of XeN_8 that this charge transfer is suppressed at 0 GPa, in line with the slight change in the 3D structure of the polynitrogen motif (fully planar at 0 GPa, corrugated at 100 GPa) and with the variations in the DOS (see S5). In both cases, the possibility to remove the Xe atoms without destruction of the polynitrogen moieties is a further indication of the limited extent of the charge transfer - which is also hinted by the NCI analysis (vide infra).

S7.2 Non-Covalent Interaction Index analysis

(a) XeN_{20} @ 0 GPa XeN_{20} @ 100 GPa

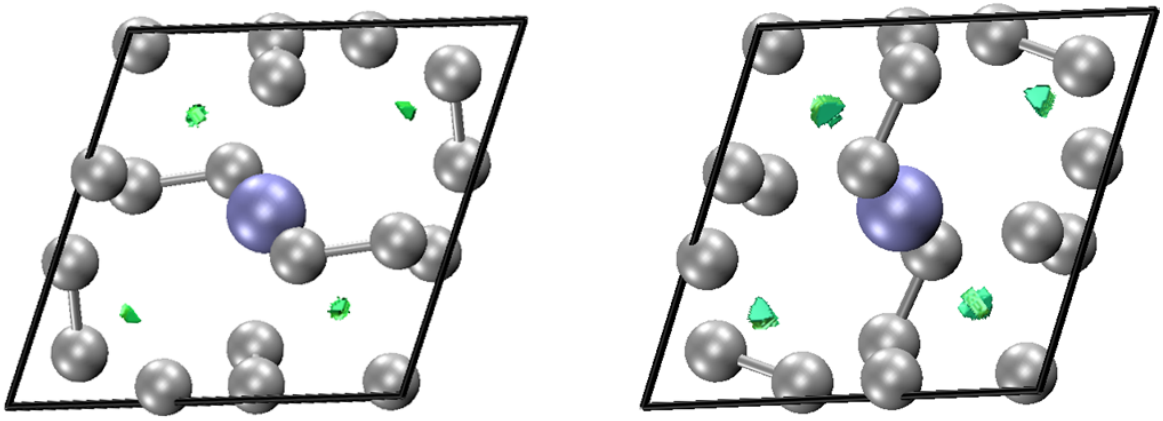

(b) XeN_{18} @ 100 GPa

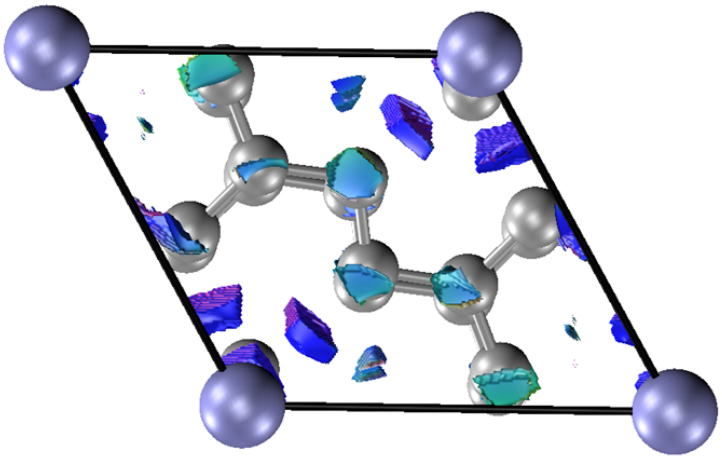

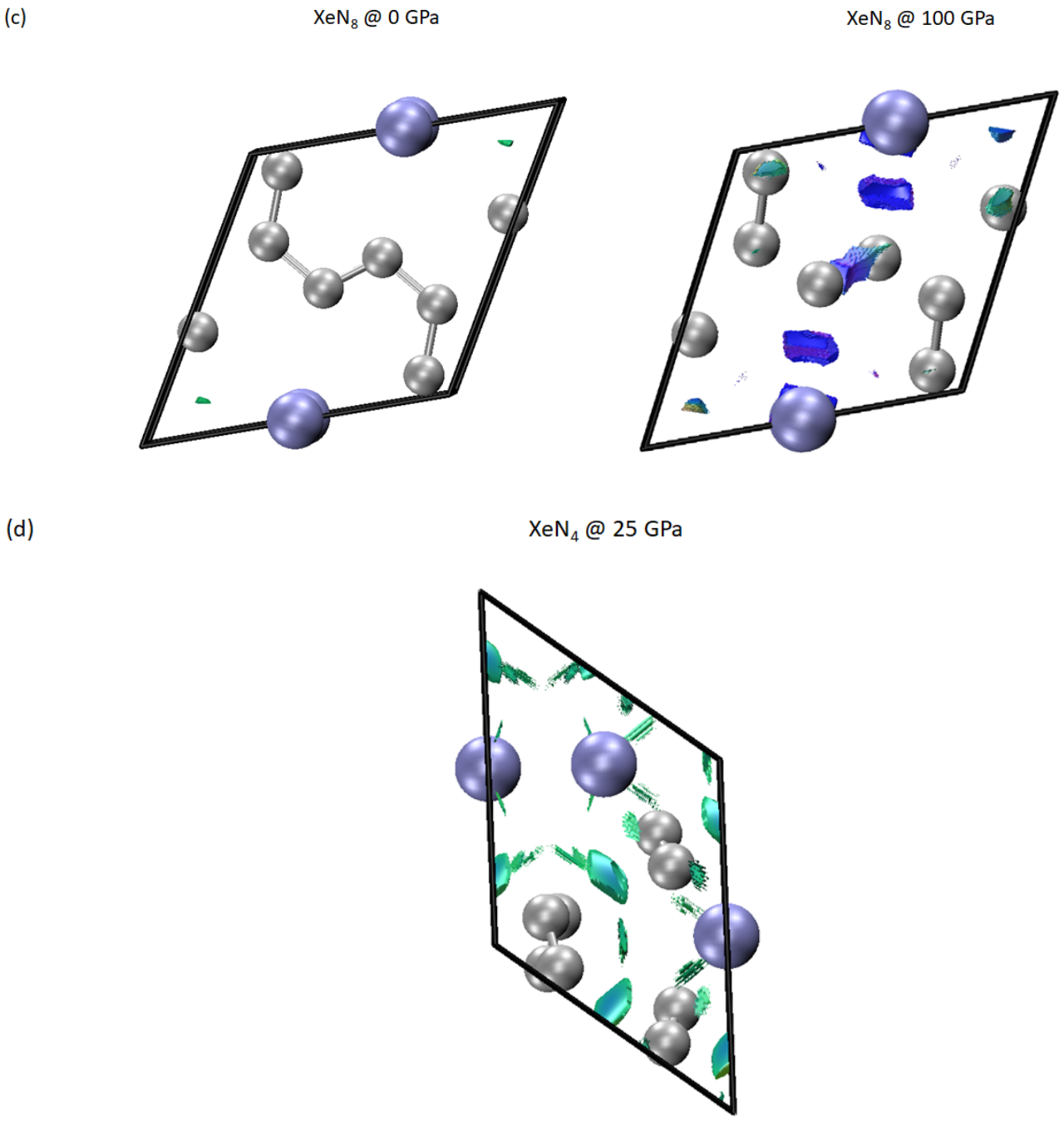

Figure S21. Reduced gradient isosurfaces (s=0.5 a.u.) for XeN_4, XeN_8, XeN_{18}, and XeN_{20} under specific pressure. Xe atoms are depicted in blue and N atoms in gray. Surfaces are colored according to the usual blue-green-red color scheme associated with the sign of the second Hessian eigenvalue (<0, blue; =0, green; >0 red). Only negative/nil values are depicted for the sake of clarity.

As shown in Figure S21, NCI analysis is in line with electron density difference maps: in most cases, only moderately stabilizing (dispersive) interactions are observed, associated to greenish volumes. Stronger interactions are observed only in the case of XeN_{18} and XeN_8 at 100 GPa, in line with the observed slight charge transfer (*vide supra*).

S8. Simulated X-ray diffraction patterns

As X-Ray diffraction (XRD) is routinely used to identify crystalline phases and can provide unit cell information, XRD spectrums were produced using VESTA software. The wavelength λ of 1.48 Å was used for XRD simulations. The calculated XRD spectrum of the *Fm*-3 XeN_{20}, *P*-1 XeN_{18}, *P*-1 $XeN_{8,}$ and $I4_1/amd$ XeN_4 are presented in Figure S22.

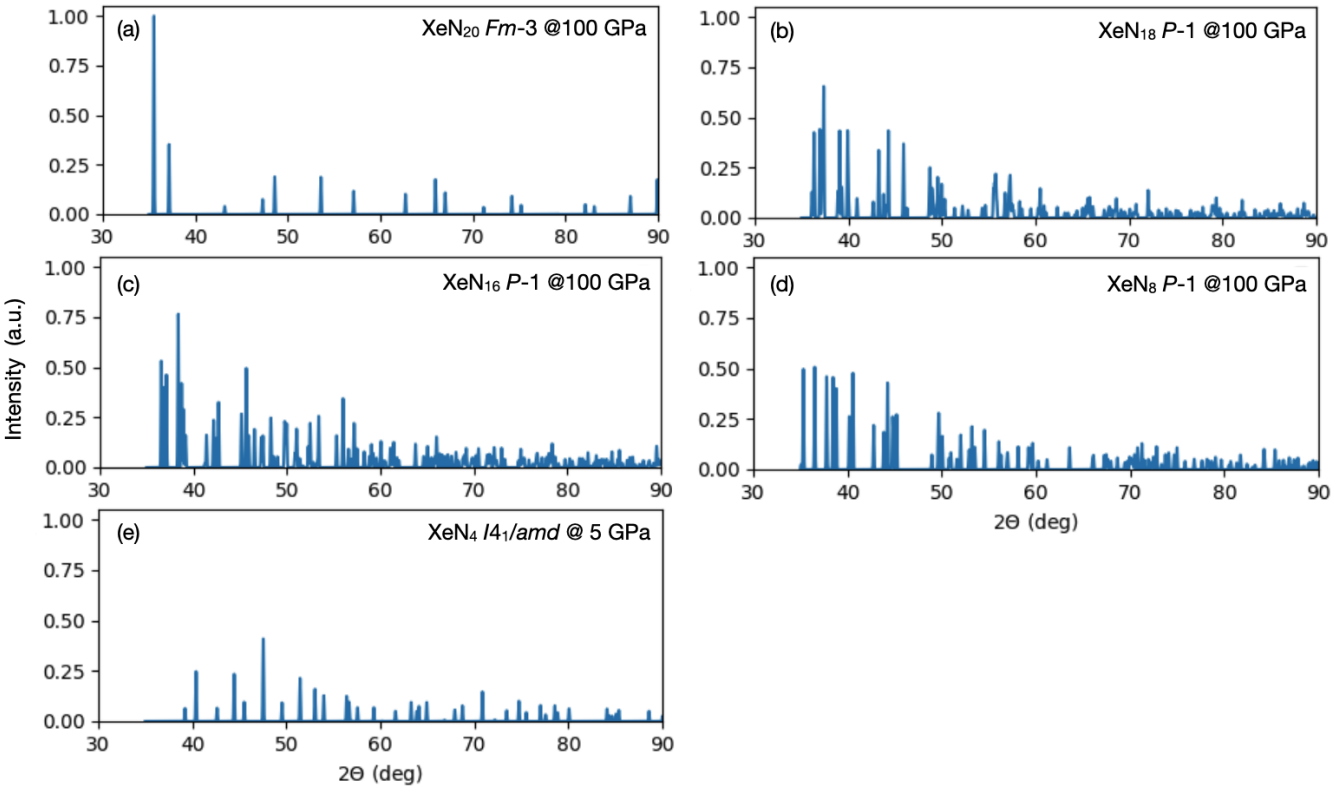

Figure S22. Calculated X-ray diffraction patterns for *Fm*-3 XeN_{20}, *P*-1 XeN_{18}, *P*-1 $XeN_{8,}$ and $I4_1/amd$ XeN_4 under specific pressure.

S9. *Fm*-3 Ng@N_{20} compounds (Ng=He, Ne, Ar, and Kr)

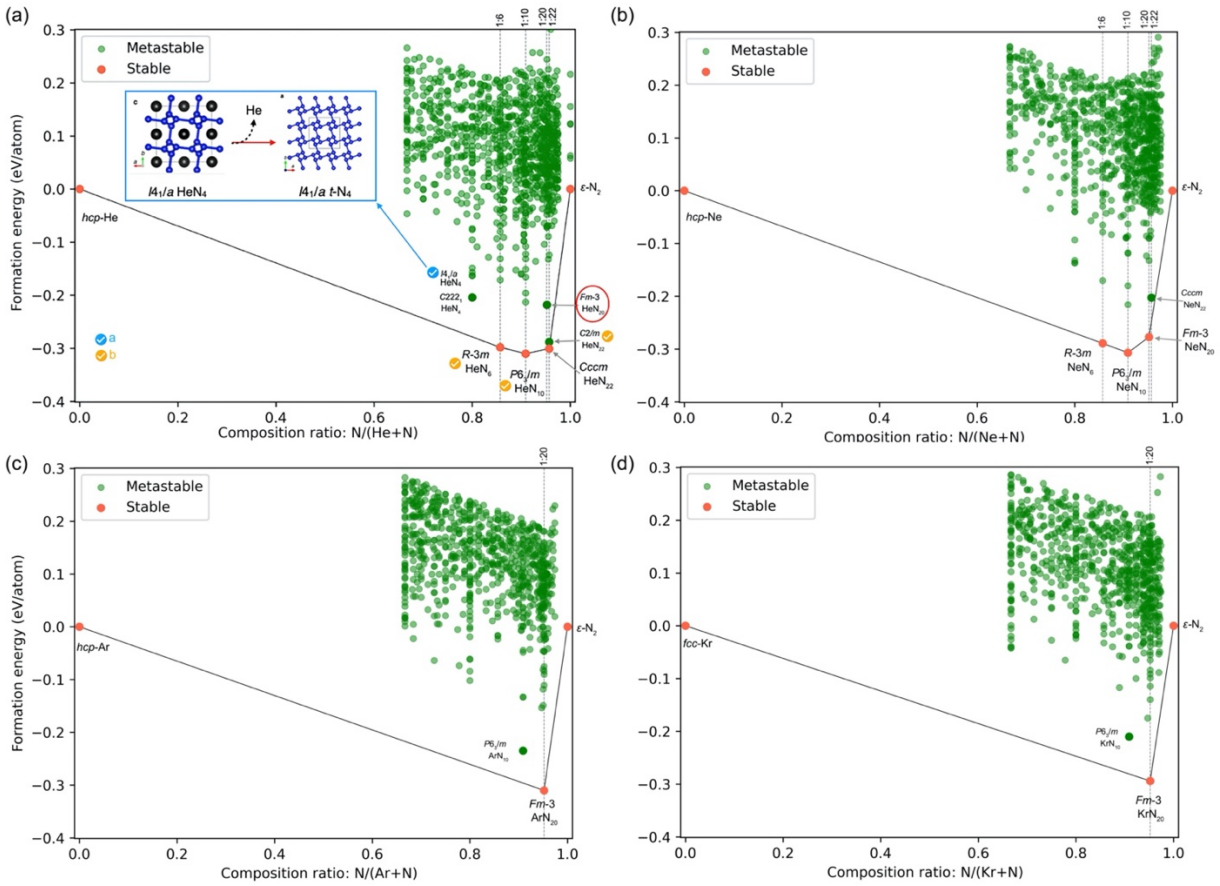

Figure S23. Convex-hull diagrams for the Ng−N system (Ng = He, Ne, Ar, and Kr) under 100 GPa with PBE level of theory. The red dots denote thermodynamic stable phases, and the green ones represent metastable structures. The space group is indicated for each novel dynamical stable structure. Here, the ε-N_2 and accordingly ground state Ng phases (*hcp*-He, *hcp*-Ne, *hcp*-Ar, and *fcc*-Kr) were used to calculate the formation enthalpies at 100 GPa and 0 K. To be noted, only the data (composition ratio > 2/3) are depicted. In (a) He-N system, the blue and yellow circles indicate the previously reported phases by Li *et. al*.[29] and Hou *et. al*.[31], respectively.

Remarkably, all the *Fm*-3 Ng@N_{20} are shown on their (ε-N_2+Ng) convex hulls at 100 GPa, except the HeN_{20}. The *Fm*-3 HeN_{20} is located at 82 meV/atom above the convex hull. Moreover, the previously reported metastable $I4_1/a$ HeN_4[29] are located above the convex hull, while the reported stable *R*-3*m* HeN_6, $P6_3/m$ HeN_{10}, and *C*2/*m* He(N_2)(N_{20}) are on the convex hull at our level of theory (PBE).[31] Interestingly, a distorted *C*2/*m* He(N_2)(N_{20}) with rotated N_2 molecular, named *Cccm* He(N_2)(N_{20}) is predicted on the convex hull in our structure searches, whose formation enthalpy is slightly (13 meV/atom) below that of reported *C*2/*m* He(N_2)(N_{20}).[31]

In the Ne-N system, the *R*-3*m* NeN_6 and $P6_3/m$ NeN_{10} crystalize in the same structure as HeN_6 and HeN_{10}. They are predicted to be the thermodynamic phases. Moreover, the *Fm*-3 NeN_{20} turns out to be on the convex hull.

For the Ar/Kr-N systems, only the *Fm*-3 ArN_{20} *and* KrN_{20} are calculated on the convex hull, as shown in Figure S23.

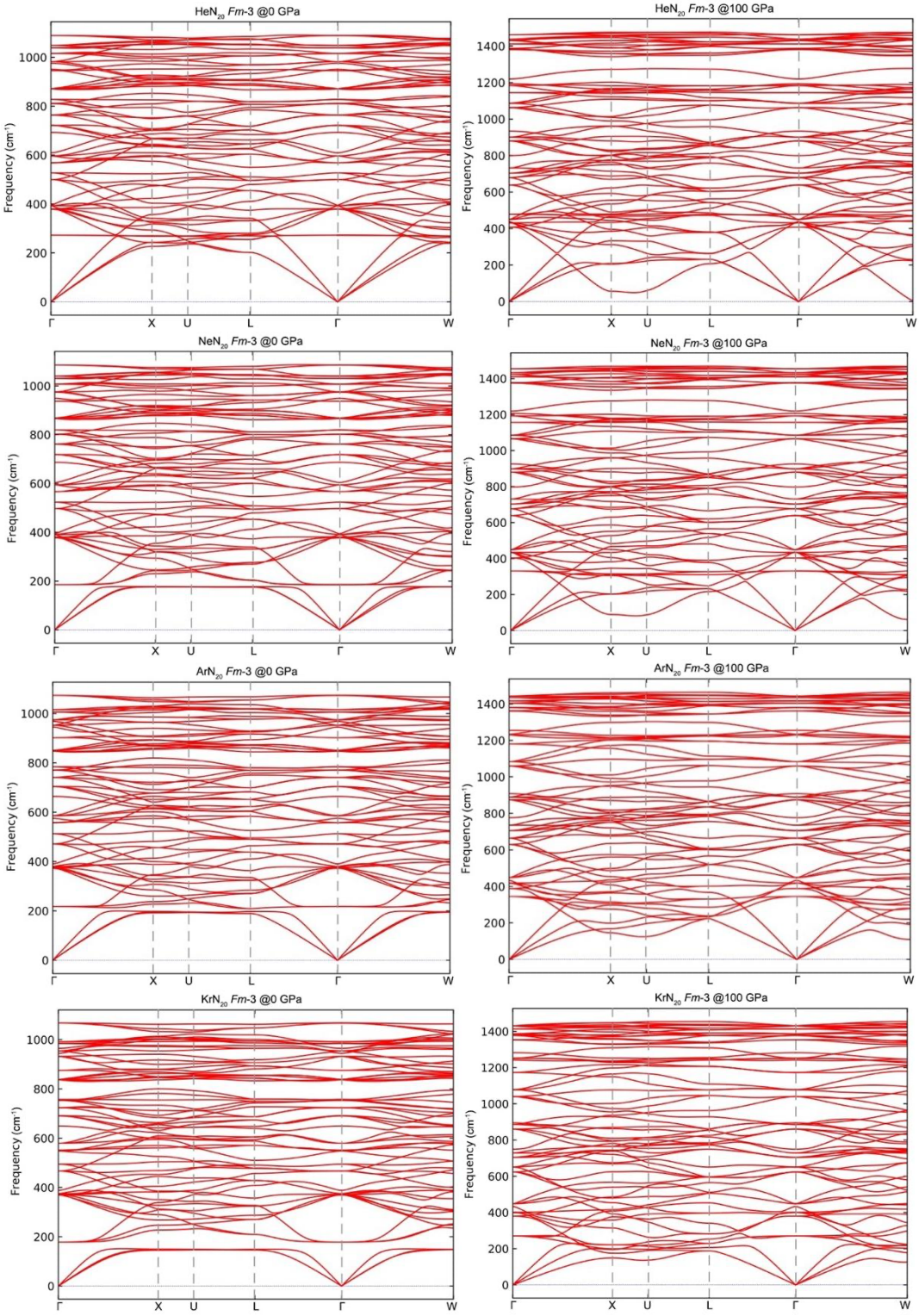

Figure S24. Phonon dispersion curves of *Fm*-3 Ng@N_{20} compounds (Ng = He, Ne, Ar, and Kr) at 0 and 100 GPa.

No imaginary phonon modes are found in the whole Brillouin zone, confirming their dynamical stability.

Table S7. Structural parameters of dynamically stable Noble-nitride phases (distances in Å, angles in °, energy in eV/atom) at the SCAN+rVV10 level of theory.

Phase	Pressure (GPa)	Space group	Z	Lattice parameters	Atomic coordinates (fractional)
KrN_{20}	100	*Fm*-3	4	a=b=c=7.953 α=β=γ=90.0	Kr (0.000, 0.000, 0.500); N (0.000, 0.222, 0.167), (0.141, 0.141, 0.141)
KrN_{20}	0	*Fm*-3	4	a=b=c=8.559 α=β=γ=90.0	Kr (0.000, 0.000, 0.500); N (0.000, 0.215, 0.169), (0.139, 0.139, 0.139)
ArN_{20}	100	*Fm*-3	4	a=b=c=7.893 α=β=γ=90.0	Ar (0.000, 0.000, 0.500); N (0.000, 0.226, 0.165), (0.141, 0.141, 0.141)
ArN_{20}	0	*Fm*-3	4	a=b=c=8.500 α=β=γ=90.0	Ar (0.000, 0.000, 0.500); N (0.000, 0.218, 0.168), (0.139, 0.139, 0.139)
NeN_{20}	100	*Fm*-3	4	a=b=c=7.790 α=β=γ=90.0	Ne (0.000, 0.000, 0.500); N (0.000, 0.231, 0.163), (0.141, 0.141, 0.141)
NeN_{20}	0	*Fm*-3	4	a=b=c=8.408 α=β=γ=90.0	Ne (0.000, 0.000, 0.500); N (0.000, 0.221, 0.167), (0.139, 0.139, 0.139)
HeN_{20}	100	*Fm*-3	4	a=b=c=7.785 α=β=γ=90.0	He (0.000, 0.000, 0.500); N (0.000, 0.232, 0.161), (0.141, 0.141, 0.141)
HeN_{20}	0	*Fm*-3	4	a=b=c=8.456 α=β=γ=90.0	He (0.000, 0.000, 0.500); N (0.000, 0.220, 0.166), (0.140, 0.140, 0.140)

S10. The effect of zero-point energy

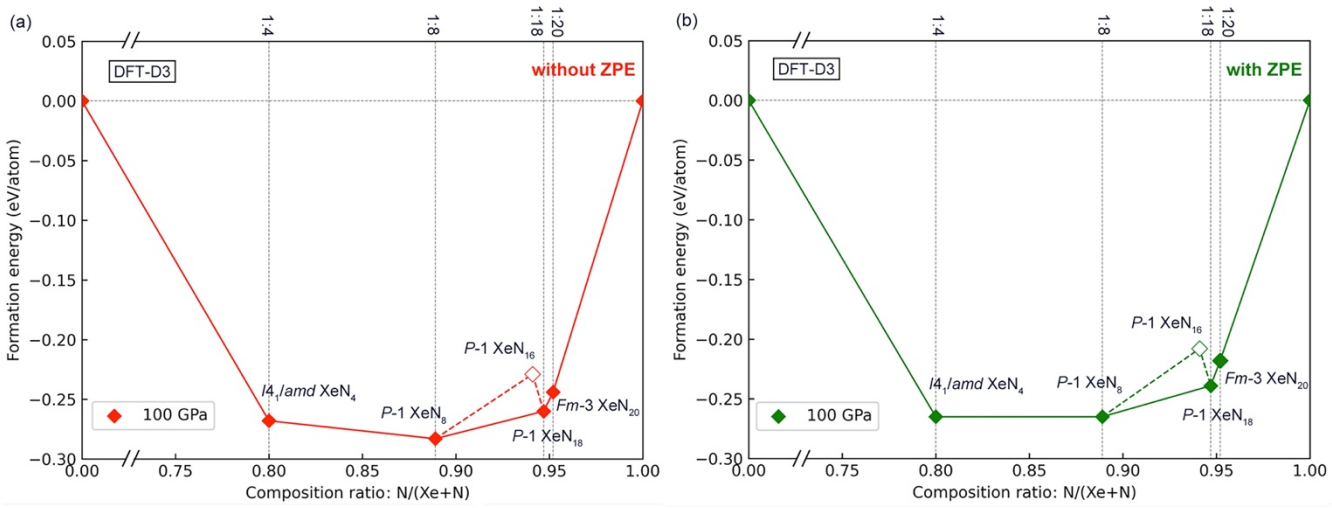

Figure S25. Convex-hull diagrams (a) without and (b) with ZPE correction (DFT-D3 level of theory) for the Xe-N system under 100 GPa regarding the *hcp*-Xe ($P6_3/m$) and ε-N_2 (R-3c).

The effect of zero-point energy (ZPE) on the stability of Xe-N compounds is studied. We find that the inclusion of ZPE only moderately shifts the stability figures but doesn't change the phase stability order.

Table S8. Calculated enthalpies of the predicted XeN_x compounds using DFT-D3.

Structure	Space Group	Pressure (GPa)	ZPE (eV/atom)	Enthalpy with ZPE (eV/atom)	Formation Enthalpy with ZPE (eV/atom)
Xe	$P6_3/m$	100	0.037	16.077	0.000
XeN_4	$I4_1/amd$	100	0.119	0.871	-0.264
XeN_8	P-1	100	0.143	-0.789	-0.265
XeN_{16}	P-1	100	0.151	-1.708	-0.208
XeN_{18}	P-1	100	0.152	-1.855	-0.239
XeN_{20}	Fm-3	100	0.158	-1.928	-0.218
ε-N_2	R-3c	100	0.136	-2.599	0.000

S11. References

(1) Oganov, A. R.; Glass, C. W. Crystal Structure Prediction Using Ab Initio Evolutionary Techniques: Principles and Applications. *J. Chem. Phys.* **2006**, *124* (24), 244704.

(2) Oganov, A. R.; Lyakhov, A. O.; Valle, M. How Evolutionary Crystal Structure Prediction Works—and Why. *Acc. Chem. Res.* **2011**, *44* (3), 227–237.

(3) Lyakhov, A. O.; Oganov, A. R.; Stokes, H. T.; Zhu, Q. New Developments in Evolutionary Structure Prediction Algorithm USPEX. *Comput. Phys. Commun.* **2013**, *184* (4), 1172–1182.

(4) Zhou, X.-F.; Dong, X.; Oganov, A. R.; Zhu, Q.; Tian, Y.; Wang, H.-T. Semimetallic Two-Dimensional Boron Allotrope with Massless Dirac Fermions. *Phys. Rev. Lett.* **2014**, *112* (8), 85502.

(5) Kresse, G.; Furthmüller, J. Efficient Iterative Schemes for Ab Initio Total-Energy Calculations Using a Plane-Wave Basis Set. *Phys. Rev. B* **1996**, *54* (16), 11169–11186.

(6) Kresse, G.; Furthmüller, J. Efficiency of Ab-Initio Total Energy Calculations for Metals and Semiconductors Using a Plane-Wave Basis Set. *Comput. Mater. Sci.* **1996**.

(7) Blöchl, P. E. Projector Augmented-Wave Method. *Phys. Rev. B* **1994**, *50* (24), 17953–17979.

(8) Kresse, G.; Joubert, D. From Ultrasoft Pseudopotentials to the Projector Augmented-Wave Method. *Phys.Rev.B* **1999**, *59*, 1758.

(9) Perdew, J. P.; Burke, K.; Ernzerhof, M. Generalized Gradient Approximation Made Simple. *Phys. Rev. Lett.* **1996**, *77* (18), 3865–3868.

(10) Perdew, J. P.; Burke, K.; Ernzerhof, M. Erratum: Generalized Gradient Approximation Made Simple. *Phys. Rev. Lett.* **1997**, *78*, 1396.

(11) Sabatini, R.; Gorni, T.; De Gironcoli, S. Nonlocal van Der Waals Density Functional Made Simple and Efficient. *Phys. Rev. B* **2013**, *87* (4), 41108.

(12) Peng, H.; Yang, Z.-H.; Perdew, J. P.; Sun, J. Versatile van Der Waals Density Functional Based on a Meta-Generalized Gradient Approximation. *Phys. Rev. X* **2016**, *6* (4), 41005.

(13) Sun, J.; Ruzsinszky, A.; Perdew, J. P. Strongly Constrained and Appropriately Normed Semilocal Density Functional. *Phys. Rev. Lett.* **2015**, *115* (3), 36402.

(14) Grimme, S.; Antony, J.; Ehrlich, S.; Krieg, H. A Consistent and Accurate Ab Initio Parametrization of Density Functional Dispersion Correction (DFT-D) for the 94 Elements H-Pu. *J. Chem. Phys.* **2010**, *132* (15), 154104.

(15) Heyd, J.; Scuseria, G. E.; Ernzerhof, M. Hybrid Functionals Based on a Screened Coulomb Potential. *J. Chem. Phys.* **2003**, *118* (18), 8207–8215.

(16) Momma, K.; Izumi, F. VESTA: A Three-Dimensional Visualization System for Electronic and Structural Analysis. *J. Appl. Crystallogr.* **2014**, 1–2.

(17) Johnson, E. R.; Keinan, S.; Mori-Sanchez, P.; Contreras-Garcia, J.; Cohen, A. J.; Yang, W. T. Density-Functional Theory, Self-Directed Growth, Electron-Density, Topological Analysis, Correlation-Energy, Proteins, Localization, Exchange, Accurate, Bonds. *J Am Chem Soc* **2010**, *132*, 6498–6506.

(18) Otero-De-La-Roza, A.; Johnson, E. R.; Contreras-Garcia, J. Revealing Non-Covalent Interactions in Solids: NCI Plots Revisited. *Phys. Chem. Chem. Phys.* **2012**, *14* (35), 12165–12172.

(19) Otero-de-la-Roza, A.; Johnson, E. R.; Luaña, V. Critic2: A Program for Real-Space Analysis of Quantum Chemical Interactions in Solids. *Comput. Phys. Commun.* **2014**, *185* (3), 1007–1018.

(20) Otero-de-la-Roza, A.; Blanco, M. A.; Pendás, A. M.; Luaña, V. Critic: A New Program for the Topological Analysis of Solid-State Electron Densities. *Comput. Phys. Commun.* **2009**, *180* (1), 157–166.

(21) Humphrey, W.; Dalke, A.; Schulten, K. VMD: Visual Molecular Dynamics. *J. Mol. Graph.* **1996**, *14* (1), 33–38.

(22) Togo, A.; Oba, F.; Tanaka, I. First-Principles Calculations of the Ferroelastic Transition between Rutile-Type and $CaCl_2$-Type SiO_2 at High Pressures. *Phys. Rev. B* **2008**, *78* (13), 134106.

(23) Howie, R. T.; Turnbull, R.; Binns, J.; Frost, M.; Dalladay-Simpson, P.; Gregoryanz, E. Formation of

Xenon-Nitrogen Compounds at High Pressure. *Sci. Rep.* **2016**, *6* (October), 2–7.

(24) Laniel, D.; Weck, G.; Loubeyre, P. Xe(N2)2 Compound to 150 GPa: Reluctance to the Formation of a Xenon Nitride. *Phys. Rev. B* **2016**, *94* (17), 1–8.

(25) Eremets, M. I.; Gavriliuk, A. G.; Trojan, I. A.; Dzivenko, D. A.; Boehler, R. Single-Bonded Cubic Form of Nitrogen. *Nat. Mater.* **2004**, *3* (8), 558–563.

(26) Gregoryanz, E.; Goncharov, A. F.; Sanloup, C.; Somayazulu, M.; Mao, H. K.; Hemley, R. J. High P-T Transformations of Nitrogen to 170 GPa. *J. Chem. Phys.* **2007**, *126* (18).

(27) Hirshberg, B.; Gerber, R. B.; Krylov, A. I. Calculations Predict a Stable Molecular Crystal of N8. *Nat. Chem.* **2014**, *6* (1), 52–56.

(28) Tomasino, D.; Kim, M.; Smith, J.; Yoo, C. S. Pressure-Induced Symmetry-Lowering Transition in Dense Nitrogen to Layered Polymeric Nitrogen (LP-N) with Colossal Raman Intensity. *Phys. Rev. Lett.* **2014**, *113* (20), 1–5.

(29) Li, Y.; Feng, X.; Liu, H.; Hao, J.; Redfern, S. A. T.; Lei, W.; Liu, D.; Ma, Y. Route to High-Energy Density Polymeric Nitrogen t-N via He-N Compounds. *Nat. Commun.* **2018**, *9* (1), 1–7.

(30) Bondarchuk, S. V. Bipentazole (N10): A Low-Energy Molecular Nitrogen Allotrope with High Intrinsic Stability. *J. Phys. Chem. Lett.* **2020**, *11* (14), 5544–5548.

(31) Hou, J.; Weng, X.; Oganov, A. R.; Shao, X.; Gao, G.; Dong, X.; Wang, H.; Tian, Y.; Zhou, X. Helium-Nitrogen Mixtures at High Pressure. *Phys. Rev. B* **2021**, *103* (6), L060102.

(32) Ji, C.; Ji, C.; Adeleke, A. A.; Yang, L.; Wan, B.; Gou, H.; Yao, Y.; Li, B.; Meng, Y.; Smith, J. S.; Prakapenka, V. B.; Liu, W.; Shen, G.; Mao, W. L.; Mao, H. K. Nitrogen in Black Phosphorus Structure. *Sci. Adv.* **2020**, *6* (23), 1–8.

(33) Laniel, D.; Winkler, B.; Fedotenko, T.; Pakhomova, A.; Chariton, S.; Milman, V.; Prakapenka, V.; Dubrovinsky, L.; Dubrovinskaia, N. High-Pressure Polymeric Nitrogen Allotrope with the Black Phosphorus Structure. *Phys. Rev. Lett.* **2020**, *124* (21), 216001.